We are IntechOpen, the world's leading publisher of Open Access books Built by scientists, for scientists

6,900
Open access books available

186,000
International authors and editors

200M
Downloads

Our authors are among the

154
Countries delivered to

TOP 1%
most cited scientists

12.2%
Contributors from top 500 universities

CLARIVATE ANALYTICS
BOOK CITATION INDEX
INDEXED

WEB OF SCIENCE™

Selection of our books indexed in the Book Citation Index
in Web of Science™ Core Collection (BKCI)

Interested in publishing with us?
Contact book.department@intechopen.com

Numbers displayed above are based on latest data collected.
For more information visit www.intechopen.com

A Study on Design of
Fiber-Reinforced Plastic (FRP) Tubes
as Energy Absorption Element in Vehicles

Yuqiu Yang and Hiroyuki Hamada
Kyoto Institute of Technology
Matsugasaki, Sakyo-ku, Kyoto
Japan

1. Introduction

To date, the global automotive industry is arguably the largest and most complex undertaking in industrial history. However, where cars multiply twice as fast as people, the automobile accidents old as automobiles themselves increased correspondingly. A car accident is a road traffic incident which usually involves at least one road vehicle being in collision with which may result in injury, property damage, sometimes even death at serious situations. Up to now, road traffic injuries represent about 25% of worldwide injury-related deaths as the leading cause. Facing the transport safety problem, policymakers in government of all over the world are doing their efforts e.g. NHTSA of USA. On the other hand, the automakers are also putting their emphasis in the increasing of the production quality particularly their crashworthiness and crash compatibility. Till now, many products including bumper, seat belt, airbag, anti-lock braking system (ABS) are proved useful to secure the occupant from a collision or a sudden stop and therefore already required as the mandatory equipments. Additionally, for scientists and engineers, in the late of 1990's, a particular international conference and a journal publication on crashworthiness well known as ICRASH and IJCRASH were formed and provide them a platform to discuss and present their works in the field of structural crashworthiness and impact biomechanics. Besides safety, the automobile have another serious problem i.e. pollution. Most automobiles in use today are propelled by gasoline or diesel. When it runs on the road, it creates a lot of exhaust gas such as NO_x that pollute the air and CO_2 which is one major causes of global warming. With the increasing demands both for energy and environment protection, economic cooperation (ECO) cars which have high fuel efficiency therefore are desirable. It is considered that the improvement of the fuel efficiency can be realized by reducing the vehicle's weight. For a traditional metallic vehicle, however, it is difficult to realize both light weight and high crashworthiness. Therefore, people are considered use new materials system to instead of metal to manufacture next generation automobile. In the area, fiber reinforced composites (FRPs) are found to be attractive [1-28].

Research into the use of structural components such as bumper for energy management is not new. As a result, the energy absorbing characteristics of metals are fairly well understood. However, until the late 1970's, attempts at understanding the energy absorbing capabilities

and crushing mechanisms of FRPs have been made [1-4]. Most of the existing work on the energy absorption capability of FRPs has concentrated on the behaviors of the tubular specimens. In general, FRP tubes do not exhibit the ductile failure mechanism associated with metals. Instead, the brittle nature of most fibers tends to generate a brittle mode of failure. That is to say unlike metals, which absorb energy through plastic deformation, most FRP tubes are found to absorb energy through progressive crushing mode by a combination of multi micro-fracture and friction [5-10]. It is this fundamental difference which gives rise to the very distinct energy absorption characteristics of FRPs. As the above researched showing, the energy absorption capacity of FRP tubes is more attractive than metals. However, the adoption of composite as energy absorbing structural elements is limited at present. There are many main reasons. One of them is that the crushing performances and the energy absorption mechanisms of FRP tubes are complicated as compared to metal. Referring to the energy absorption capability, there are many important variables. Although a lot of researches have been done on the inhere materials (reinforced fiber, matrix and the bonding between them) [5, 10, 11-15] and the reinforcement form (roving, cloth, braiding, knitting, chopped, and so on) [16-24], there is still an urgent need of database from various composite tubes and a complete understanding of the energy management from the multi micro fractures. Secondly, the manufacturing cost of a FRP tube is rather higher than that of metal. Cost is considered to be the key to apply the FRP into practice. Therefore the effects on the cost down are always warm welcome. Additionally, research on actual application of composites is absent. Apart from the understanding of the energy absorption capacity of the FRP tubes, a reasonable design such as the geometry, length, located position and collapse trigger is required to transcend the experimental stage and cross over to true application studies. Therefore, current studies elaborate some experiments on this aspect. Three improvement methods including the design of the bending energy of the tube fronds and the design of the fiber fractures energy were proposed. Firstly, in this paper, the crushing behavior of FRP tube was linked with the appearance of the bending behavior of beam. Then mechanism model of a bending beam was used to simulate the bending fronds of FRP tube. Based on the founding that the bending energy is related directly to the geometry of transversal cross section, design of the bending energy though the design of the geometry of the FRP tubes was carried out. In details, a FRP tube with general square transversal cross section was designed to mimic the circular one through applying a big radius on the corners. Additionally, a special shape which utilizing both circular and square geometry in transversal cross section was designed.

Up to now, much of the preceding discussion on the energy absorption capability of FRP tubes had been carried out to investigate the effects of the internal components and the structures. At the same time, researchers have found that the energy management has been shown to be dependent on a number of external factors, for example, strain rate i.e. crushing speed and collapse trigger mechanism. The influence of strain rate would appear to be one of the most contentious issues relating to the energy absorption of FRPs [6,9,13,28,30-35]. As an energy absorption element in automobiles, the crushing performance and the energy management in dynamic condition is eagerly to be clarified. However, until now there is not a clear understanding about the relationship between the energy management and crushing speed. Some authors have reported increases in specific energy absorption (Es, i.e. the absorbed energy per unit mass of the material) with loading rate, others decreases. Farley [30] observed a rise in specific energy absorption of up to 35% for carbon-epoxy tubes over a range of crushing speeds between 0.01 m/s and 12 m/s. However, the energy absorption of carbon-epoxy tubes with a structure of $[0/\pm\theta]^2$ was not found to be sensitive to crushing speed and

showed no increase. He suggests that energy absorption dependence on crushing speed will be related to the energy absorbing mechanism which controls the crushing process. If the mechanism is a function of strain rate then energy absorption will be a function of crushing speed. Hull [6] supported results of the increased energy management under impact test and suggested that friction in the crush zone may be another reason why energy absorption varies with crushing speed. It has been found that frictional effects generate a considerable amount of heat and it is likely that the magnitude of energy absorbed by this mechanism will vary with loading rate. Conversely, Mamalis et al. [28,31] report that the energy management of thick walled random chopped glass mat / polyester tubes exhibited a clear decrease under high speed crushing (up to 24 m/s). However, there was no clear evidence of such a decrease for thin-walled (< 4 mm tubes). Similarly to Farley [1], Mamalis et al [28] attribute the differences in energy absorption under static and dynamic conditions to the changes in the crushing mechanisms. In particular, the resin was found to become increasingly brittle under elevated strain rates. Schmueser & Wickcliffe [13] also report that energy management decreased in dynamic (5-6m/s) tests than in comparable static ones for carbon-epoxy, glass-epoxy and aramid-epoxy tubes. In some cases, dynamic energy absorption was only approximately 75% of equivalent static values. Although the above observations may at first sight appear contradictory, it should be recognized that they are all based on isolated examples of specific material and geometric configurations. As such, it is difficult to draw any overall conclusions. In general, the effect of strain rate on the energy absorption capability of a given composite structure is likely to be a complex function of the particular material system, fiber orientation, geometry employed and other external factors.

On the other hand, FRP tubes, no matter which components are contained, what configuration of the fibers is, or under which crushing speed, generally need a collapse trigger to trigger progressive crushing rather than a sudden catastrophic type of failure. Progressive crushing is a typical crushing performance of FRP materials in which the crushing load keeps almost constant during the whole compression process with a relative high value. However, before progressive crushing forms, there is another important stage, i.e. the initial crushing period, although the energy absorption during the initial period some times are ignored in rough calculation the *Es* values. In the case of without any trigger, the crushing load of FRP tube increases linearly in initial compression stage. When the crushing load exceeds the critical strength of the whole tube, catastrophic failures occurs. Several previous studies have investigated such collapse trigger with some modification at one end of the tube [3,5,36-39] and found that they performed well in initiating progressive crushing. The collapse trigger mechanism is to generated high stress concentration at the modified part from where the fracture is initiated or triggering before the load increase to the critical strength of the whole tube. Defects of the above triggers are involved extra cost and difficulty during the assembling procedure because of the angular edge.

2. Foundation thinking for optimization design

2.1 Bending energy

Based on the accident data analysis, it is known that about 70% accidents are from the full lap and offset impacts. Therefore, such a design of energy absorption structures is carried on in order to realize the minimum deformation of the cabin for saving the occupant's space and a small accelerate when vehicles are involved in crashes. In particular, a tubular component, termed "Front Side Member"(Fig. 1), is designed to be installed behind the

bumper as a special kind of energy absorption element which can absorb most of the impact energy through the fracture of itself in the chapter in particularly.

For a FRP tube which was fractured through progressive crushing mode, the energy absorbing mechanism can be clarified from the observation on the axial cross sections through the crush zone. Based on the summarized the observation results from the above reference papers, it is found that FRP absorb energy by multi micro-fractures. A sample cited from [12, 25] is given in Fig.2. The tube wall was split into pieces of fronds and bend to both sides of the tube. A wedge of debris was formed by the fractured fiber and resin. Under the wedge of debris, a central crack propagated. In the bending fronds, the delaminations and the fiber fractures can be observed. Based on the observations, the total absorbed energy (U_T) is considered using formulation (1).

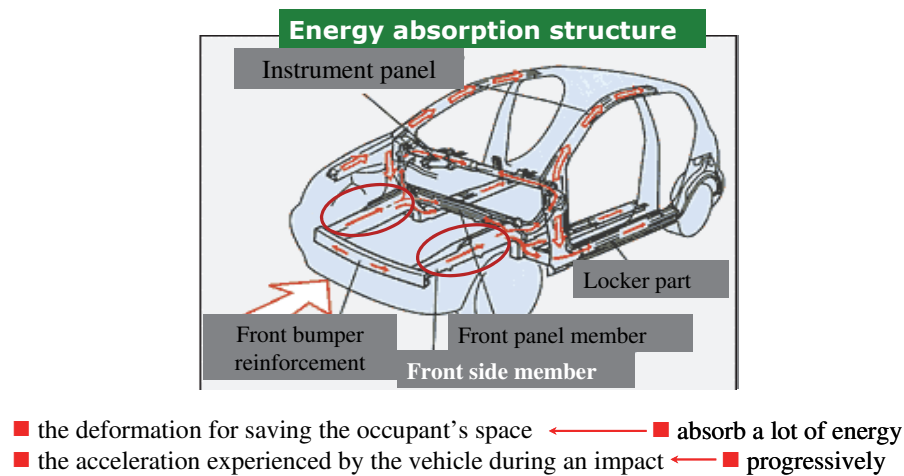$$U_T = U_{split} + U_{cc} + U_{de} + U_{bend} + U_{ff} + U_{fr} \qquad (1)$$

Fig. 1. Schematic illustration of energy absorption structure in a vehicle illustrating the component of front side member
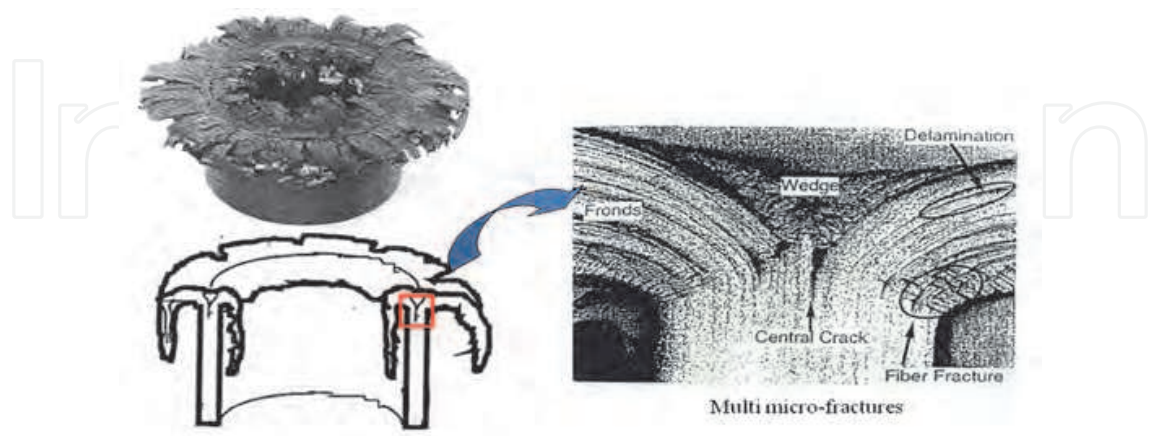

Fig. 2. Observation results on a carbon/PEEK circular tube illustrating multi micro fractures (cite from reference list [12, 25])

Here, U_{split} is the energy absorbed by splitting the integrated tube wall into pieces of fronds. U_{cc} is the energy for initiation and propagation of the central crack; U_{de} is the energy for

delaminations; U_{bend} is the energy of the bending of fronds; U_{ff} is the energy required for fiber fracture and U_{fr} is the energy associated with friction. Because these fractures occur simultaneously and they correlate and affect each other, it is difficult to evaluate individual energy absorption contribution and construct a design criterion.

In these multi-micro fractures, it is noticed that the FRP tubes show the bending behavior as the essential performance. The propagation of the central crack or delaminations and the fracture of the fibers or resin are considered to be generated during the bending process. Therefore, a solution for the design of FRP tube's energy management was proposed though design U_{bend}. Here the bending frond is considered as a bending beam by an external force. The mechanism model for such a beam with a height of l which is pulled by an external force F is illustrated in Fig.3. The displacement along longitudinal direction is the s and the y_{max} is the maximum distance in y direction. The deformation energy i.e. the bending energy U_{bend} can be express by formula 2.
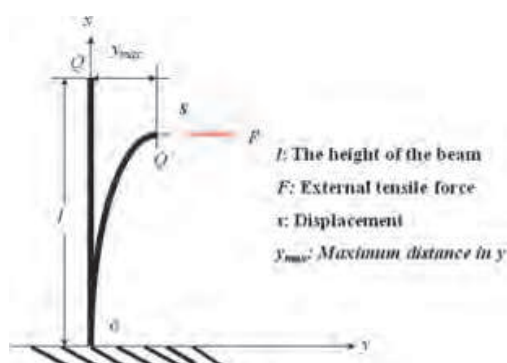

Fig. 3. Mechanism model for a beam which is pulled by an external force.

$$U_{bend} = \int_0^l \frac{M^2(x)}{2EI} dx \qquad (2)$$

Here M is the bending moment of the beam (y trial) and x is any point in x direction from 0 to s displacement. According to the relationship between external force F and y_{max} and the relationship between displacement s and maximum distance y_{max}, the bending energy can be express by formula 3. For the given material (with a modulus E and a height l) bent to a displacement compression (s), the bending energy U_{bend} is affected directly by the inertia moment (I). In a word, U_{bend} is in a function of I.

$$\begin{aligned}
\therefore U_{bend} &= \frac{F^2}{2EI} \int_0^l (l-x)^2 dx \\
&= \frac{F^2}{2EI} \int_0^l (x-l)^2 dx \\
&= \frac{F^2}{2EI} \cdot \frac{1}{3}(x-l)^3 \Big|_l^0 \\
&= \frac{F^2 l^3}{6EI}
\end{aligned}$$

and

$$F = -\frac{3EI y_{max}}{l^3}$$

$$\therefore \quad U_{bend} = \frac{3EI(y_{\max})^2}{2l^3} = \frac{5E \cdot I \cdot s}{2l^2} \tag{3}$$

An example about the effect of cross section geometry on I is given in Fig.4. For a given material with the same section area ($A:50mm^2$) and thickness ($t:4mm$), making the structure to have cross section geometry in corner or flat wall shape, different I would be obtained. Here the calculation method of I should be noted. In Fig.4(a), corner geometry is illustrated (A: cross section area of $50mm^2$; R: radius of outside of corner 10mm; r: radius of inside of corner 6mm; t: thickness 4mm). It is assumed to be split to two parts as outer and inner fronds during compression process along the broken line located in the middle of the thickness. The I of the corner region, i.e. I_{corner} can be calculated by formulae (4) and (5)

$$I_{corner} = I_{zc(outer\ frond\ in\ corner\ geometry)} + I_{zc(inner\ fornd\ in\ corner\ geometry)} \tag{4}$$

$$I_{zc(outer/inner\ frond\ in\ corner\ geometry)} = \frac{\pi+2}{16}(R^4 - r^4) - \frac{8(R^3 - r^3)^2}{9\pi(R^2 - r^2)} \tag{5}$$

Here, R and r are the radii of the curvatures of the corner. Therefore, r plus thickness (t) amounts R. Additionally, for flat wall geometry (Fig.3b, A: cross section area of $50mm^2$; t: thickness 4mm; w: length 12.5mm), the I of flat wall, i.e. $I_{flat\ wall}$ also can be calculated by (6) and (7)

$$I_{flat\ wall} = 2(I_{zc(outer\ frond\ in\ flat\ wall\ geometry)}) = 2(I_{zc(inner\ fornd\ in\ flat\ wall\ geometry)}) \tag{6}$$

$$I_{zc(outer/inner\ frond\ in\ flat\ wall\ geometry)} = \frac{1}{12}wt^3 \tag{7}$$

From the calculation results listed in the table in Fig.4(c), it is understood that I_{corner} ($40mm^4$) is bigger than $I_{flat\ wall}$ ($16.8mm^4$), although they have same cross section area and thickness. According to formula (3), under the same displacement (s), big bending energy would be generated in the structure which has the transverse cross section in corner geometry.

From previous experiences [7, 26-29], it is reported that square or rectangular tubes are generally less effective at absorbing energy than a comparable circular tube. However, square or rectangular tubes have the geometrical advantage because their flat wall can assembled with other component easily. A pure circular tube can be considered as a combination of four pieces of corner geometry while a pure square or rectangular tube consists of four pieces of flat wall regions in cross section. I of pure circular tube is quite different with that of a pure square tube even they have same cross section area and height. It is considered that much big I in circular geometry is one of the reasons why circular tube have higher energy absorption capability as compared to square tube. Based on the above thinking, therefore, the following methods were proposed aiming improved the energy absorption capacity of square and rectangular tubes, which would be designed to have reasonable consisting of 4 pieces of flat wall and 4 corners in the transversal cross section.
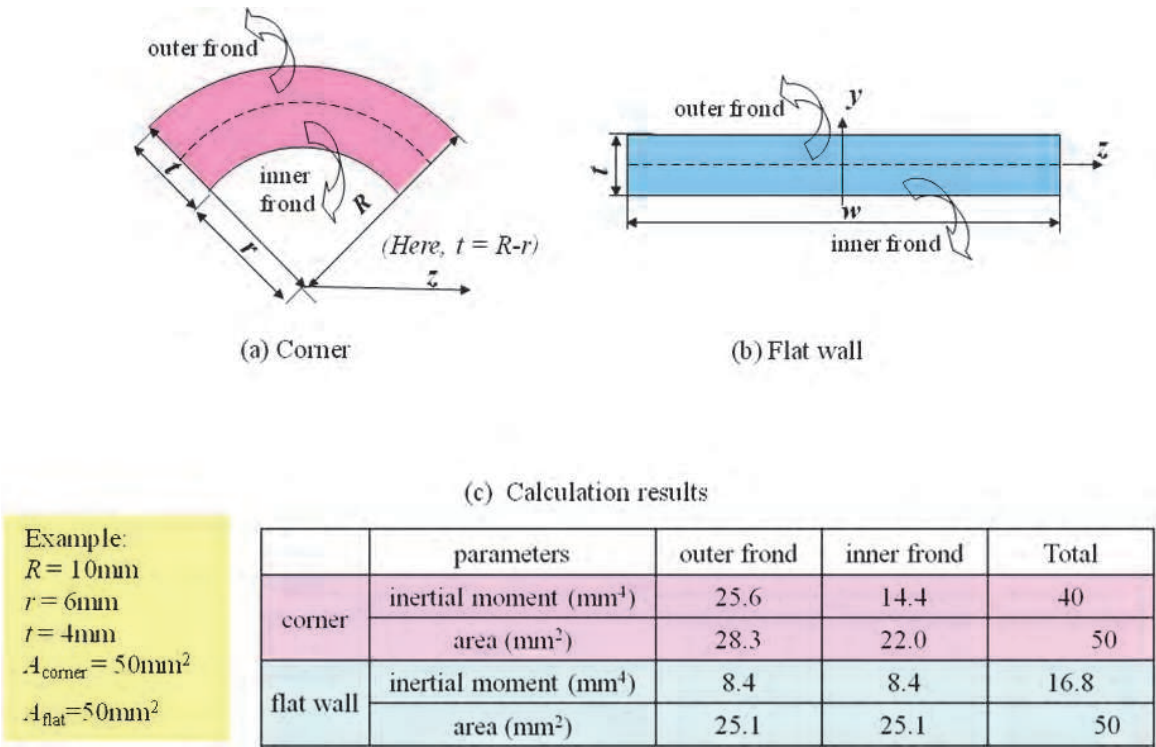
(a) Corner   (b) Flat wall

(c) Calculation results

Example:
$R = 10$mm
$r = 6$mm
$t = 4$mm
$A_{corner} = 50$mm^2
$A_{flat} = 50$mm^2

	parameters	outer frond	inner frond	Total
corner	inertial moment (mm^4)	25.6	14.4	40
	area (mm^2)	28.3	22.0	50
flat wall	inertial moment (mm^4)	8.4	8.4	16.8
	area (mm^2)	25.1	25.1	50

Fig. 4. Calculation of Inertial moments (*I*) of different geometries (A: cross section area; R: radius of outside of corner; r: radius of inside of corner; t: thickness)

2.2 Fiber fracture energy

Many researches indicated that FRP tubes absorb energy by multi micro-fractures. During the initial compression stage, a wedge of debris was formed by the fractured fiber and resin. Under the wedge of debris, a central crack propagated. Then the tube wall was split into pieces of fronds and bend to both sides of the tube (two-side-bending) along the central crack. During the bending process, delaminations and the fractures of both fiber and resin generate simultaneously. These fractures occur at the same time and they correlate and affect each other, which lead to the complication in designing the energy management. In this study, based on the consideration that the energy absorbed by fiber fractures (U_{ff}) can contributed to the total absorbed energy (U_T) significantly, an attempt to design of U_{ff} is carried out. From mechanism fracture theory, it is known that fiber fracture is affected by stresses (σ) directly. Therefore, a method to increase σ of the fronds during bending process was proposed as illustrated in Fig.5. According to equation 8, an increased thickness and a small bending curvature are helpful to obtain a high σ.

$$\sigma = \frac{E\,t}{2\,r'} \tag{8}$$

Here, E is the modulus of the composite. t and r' are the thickness and bending curvature of the bending wall, respectively. The max magnitude of these stresses (σ) can be obtained on the surfaces layers in particular bottom layers of the bending tube wall, where the radius of curvature might be smallest and the thickness largest.

Usually, the FRP tube wall, with the above mentioned collapse triggers, is split to two parts and through two-side-bending mode under the flat compression plate of testing machine to

absorb energy. At that case, before the delamination occurs, *t* is half of the tube wall. If some device can force the tube wall to be bent towards only one way (one-side-bending mode), a double thicker thickness of the frond is possible to be achieved as compared to that in two-side-bending mode. At the same time, small bending curvature could be realized through design the device. Therefore, in this study, connected with the aim of design of bending stress, device, as a new collapse trigger mechanism, is proposed. Here in this antecedent foundation investigation, the FRP tube with the transversal cross section geometry in circular and square are focused.

For the circular FRP tubes, the devices shown in Fig.6(a) are of four kinds (C-Inner 3, C-Inner 5, C-Outer 3, and C-Outer 5). The concave part of Inner type is in circular geometry with a diameter of 55mm while that of the convex part in Outer type device is 50mm. Specially, a radius (*R'*) of 3 or 5mm was modified around the circular shoulder of concave or convex part in each kind of device where the top end of the FRP tube touches the device. That is to say, the collapse of FRP tube is expected to be triggered from the *R'* region. On the other hand, S-Inner 2 (Fig.6b) was made for square FRP tube. The concave part is in a square transversal cross section with a size of 50X50mm². Similarly, a radius of 2mm (*R'2*) was chamfered on the concave part where the square end of the FRP tube contacts with it.

$$\mathbf{U_T = U_{split} + U_{cc} + U_{de} + U_{bend} + U_{ff} + U_{fr}}$$

$$U_{ff} = f(\sigma)$$

Design of σ

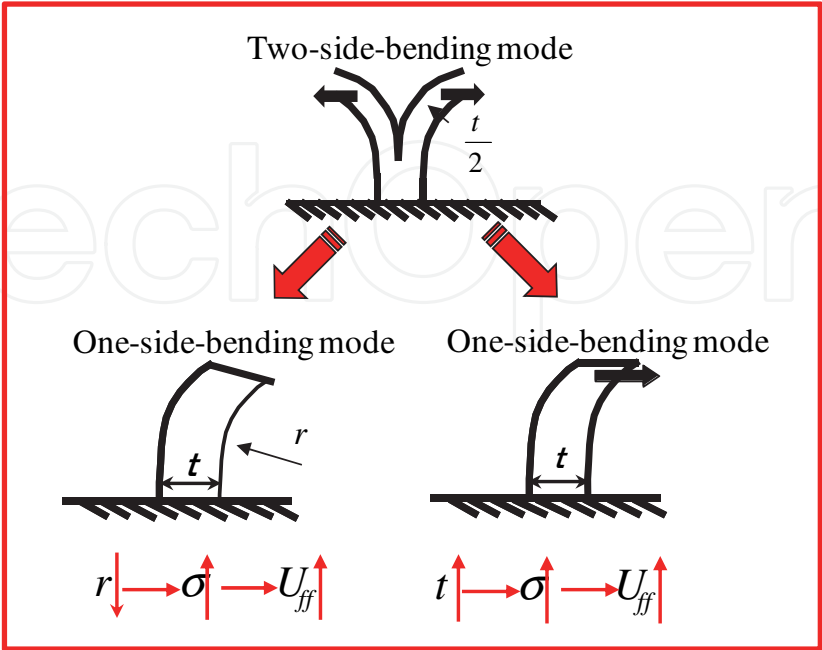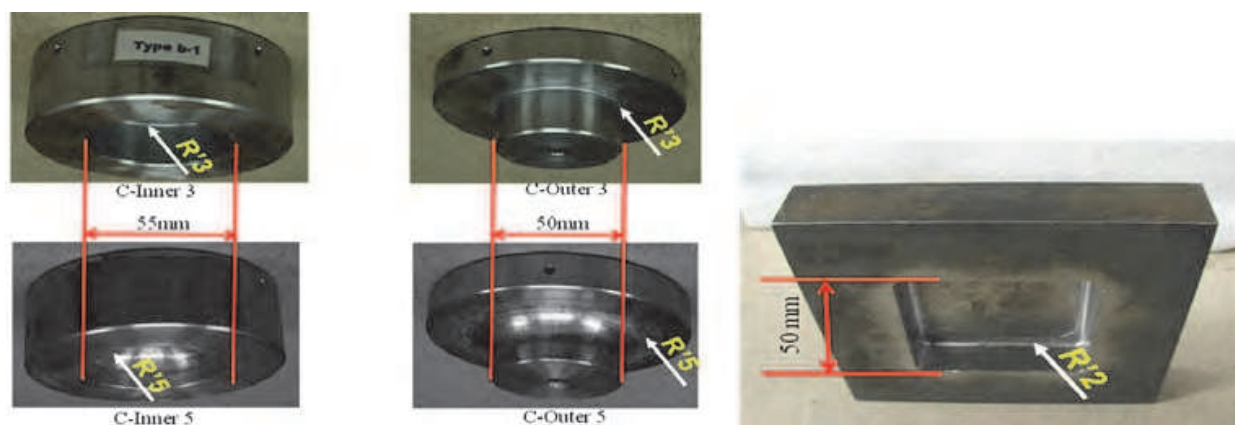$$\sigma = \frac{Et}{2r}$$

Fig. 5. Design method of fiber fracture energy

(a) four kinds of devices for circular FRP tubes   (b) S-Inner 2 devices for square FRP tubes

Fig. 6. Photographs of devices (a):four kinds of devices for circular FRP tubes illustrating the diameters of concave or convex part and the radius on the shoulder; (b) S-Inner 2 devices for square FRP tubes illustrating the size of the concave part (50X50mm²) and the radius on the shoulder.

3. Mimic of square to circular

3.1 Material and experiment

Metal mandrels with a rectangular transversal cross section of 36mmX24mm were used to fabricate the FRP tubes with a shape of rectangular in the transversal cross section. In order to investigate the effect of design of *I* of FRP tubes, two kinds of mandrels (r3 and r9 mandrels) are employed, where a radius of 3mm (r3) or 9mm (r9) was modified on the corners of the mandrel respectively.

Referring to the reinforcement form of FRP specimens in the mimic square to circular method experiments, 2.5D braids fabricated by an experimental braiding machine (Murata machinery, Ltd) were adopted. Carbon fiber (T-300 for braiding yarns and T-1000 for middle-end-fiber from Toray industries, INC.) and Epoxy (XNR 6805 from Nagase ChemteX Corporation) were used as reinforcement and matrix. 96 of the braiding yarns and 40 of middle-end-fibers were fabricated to form each layer of 2.5D braided structure given in Table 1.

The fabrication process of the braided performs includes:

1. Fabricate the preforms on the above metal mandrels according to the fiber architecture listed in Table 1.
2. Secondly, an additional braided layer was fabricated on the outside of the above preforms in order to retain the shape during subsequent impregnation process. (The additional braided layer was fabricated by traditional braiding machine with 48 bundles of braiding yarn without middle-end-yarns in a braiding angle of 60.)
3. Then these braids were impregnated with Epoxy resin by Vacuum Assisted Resin Transfer Molding process (VARTM). Finally, they were cured in an oven at 80° C for 8 hours. After cool naturally, the FRP composite tubes are drawn from the mandrels.

Depending on the mandrel shape, the carbon/epoxy braided composite tubes were divided into two groups. r3 group tubes, braided on the r3 mandrel, comprised of two different braid architectures named as r3-45 and r3-18 (45 and 18 are the value of the braiding angle). Here the braiding angle is the angle between the longitudinal axes and the braiding yarn. The r9 group tubes consisting of r9-45 and r9-18 were fabricated on R9 mandrel with the similar fiber braided architectures as r3-45 and r3-18.

The specifications of the fabricated composite tubes are summarized in Table 1.These CFRP tubes with a fiber volume fraction of about 50% were segmented into individual specimens with a length of 50mm. In order to initiate progressive crushing, one end of each specimen was chamfered to a taper with a 45 degree angle shown in Fig.7. Specially, the transversal cross section of r3 and r9 specimens are compared together to illustrate the difference in the geometry on the corners.

Quasi-static tests were performed on an INSTRON (4206) universal testing machine at a constant crosshead speed of 5.0mm/min. The composite tubes were axially crushed between parallel steel flat platens. Three replicate tests were conducted for each kind of braided composite tubes to verify the stability of the energy absorption capability. The experiment commenced when the compression platen touched smoothly the chamfered taper. Every second, five data points were recorded to follow the track of the load during the compression procedure.

		Preform		FRP tubes (2.5D braided Carbon/Epoxy)			
	specimen	Braiding angle° *	Number of layers	Thickness of long flat wall (mm)	Thickness of short flat wall (mm)	Thickness of corner (mm)	Density (g/cm³)
r3 group	r3-45	45	2	2.2	2.7	2.4	1.33
	r3-18	18	3	2.8	2.6	2.3	1.28
r9 group	r9-45	45	2	2.3	2.9	2.7	1.20
	r9-18	18	3	2.7	2.3	2.5	1.29

(Braiding angle*: the angle between the longitudinal axes and the braiding yarn)

Table 1. Specifications of carbon 2.5D braided preforms and FRP tubes which are with a rectangular transversal cross section
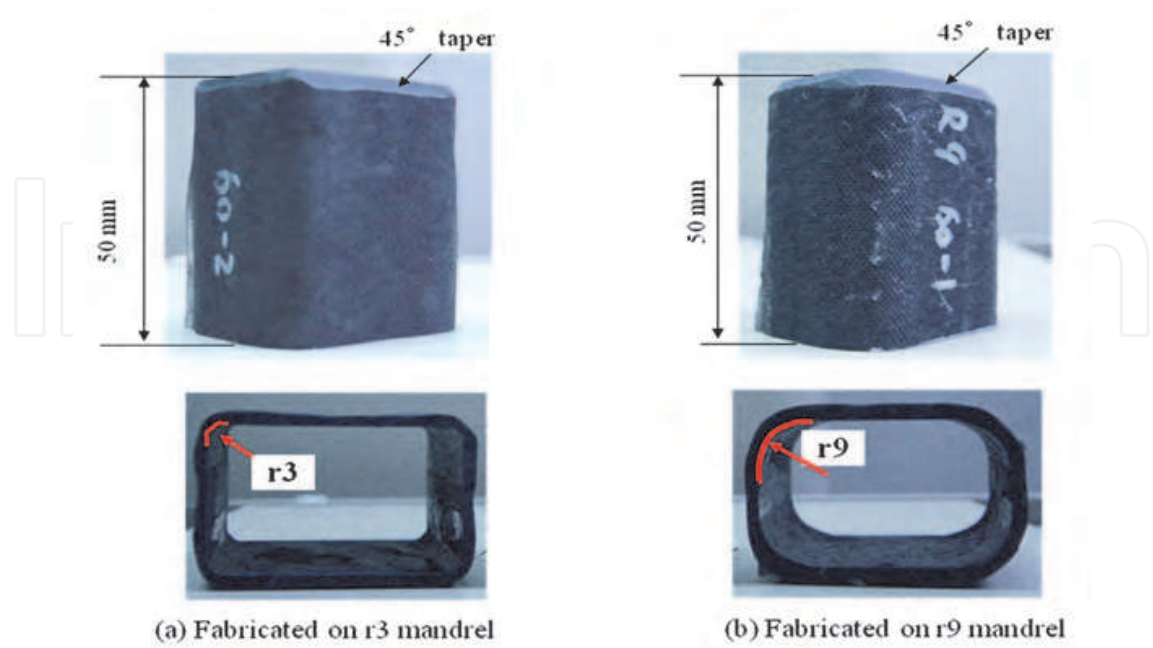

Fig. 7. Carbon fiber/Epoxy 3D braided composite tubes, illustrated the length, taper with a 45 degree angle, and corner geometry.

3.2 Results and discussion

At the initial compression stage, the taper was compressed and crushed to the inner side of the tube. With the advancement of the compression platen, the tube wall was mainly split into 4 parts along the flat wall. And each split part was bent towards both sides of the tube known as external and internal fronds. Under the compression, the split tube wall was delaminated to pieces furthermore. During the crushing procedure, a noise, that seemed to emanate from crack propagation and fractures, was heard. After approximately 30mm crushing, compression was stopped and the compression platen was returned back. The fronds sprang back with the relaxation of the compression in a way. It can be seen from Fig.8 that a wedge of debris consisting of the crushed resin and fibers formed on the top and between the external and internal fronds.
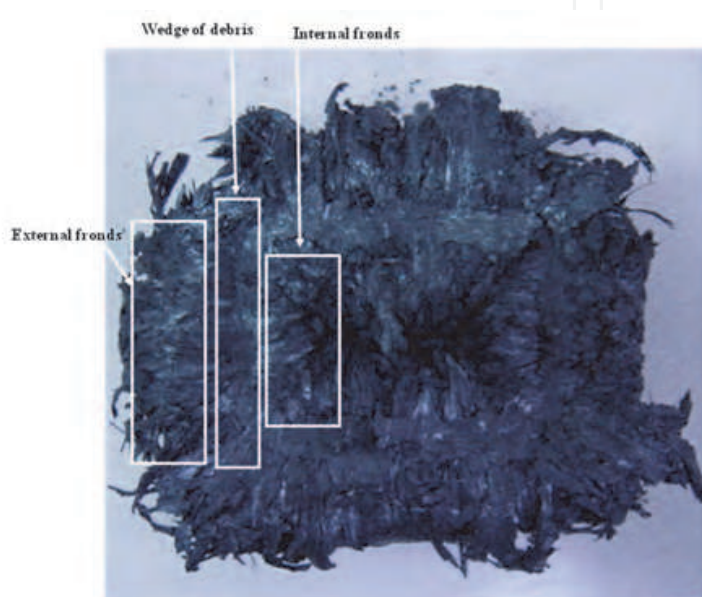
Fig. 8. Top view of the specimen after axial quasi-static compression test at a constant speed of 5mm/min. The tube was split into many parts along the flat wall and each split part includes internal and external fronds.

In order to find the difference in the crushing behavior between the r3 and r9 group tubes, the load-displacement curves of both groups are compared in Fig.9 under the same braiding angle. Here, the load per unit cross section (crushing stress) is used as the longitudinal axes to reduce the influence of thickness. For all of the specimens, a common feature of load during compression process is that the loads rapidly increased to peak at the initial stage and then show the characteristics of the progressive crushing mode. From these figures, it could be seen that the specimens fabricated on R9 mandrel achieved a relatively more stable crushing performance with a higher average stress in both of the braided texture structures. The parameters of energy absorption capability, which were calculated from the above load-displacement curves, are summarized in Fig.10. Specific energy absorption (*Es*), defined as the absorbed energy per unit mass of the crushed material, is employed to evaluate the energy absorption capacity for both groups of tubes, which is often used in the automotive industry when studying the energy absorption. Among both r3 and r9 group tubes, the *Es* values were increased with the decrease in braiding angle from 45° to 18°. With the braiding angle decreasing from 45° to 18°, the main fiber orientation is being more and more close to the axial. Longitudinal fibers sustain the axial compressive load effectively. Therefore, the

mechanical property in axial was enhanced in the tubes with a small braiding angle. Additionally, the values of *Es* of the r9 group tubes were higher as compared to that of the r3 group tubes under the same fiber architecture i.e. R9-45 and r9-18 attained about 18% and 10% higher *Es* than that of r3-45 and r3-18, respectively.
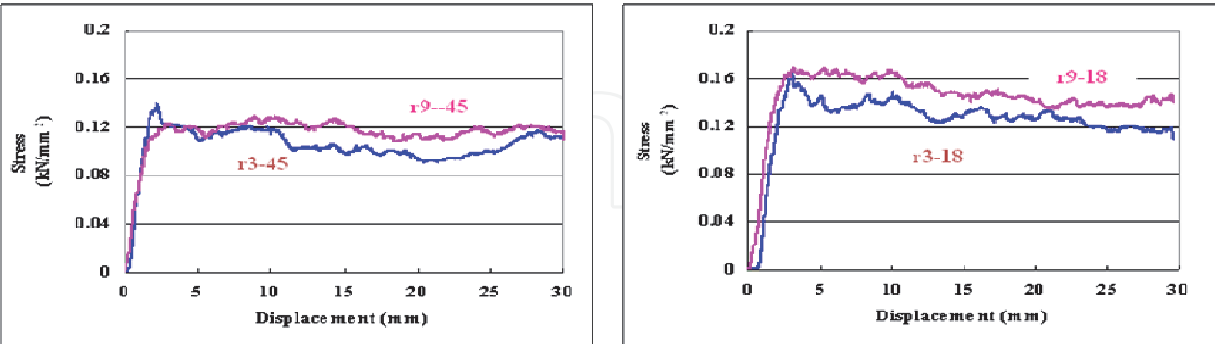

Fig. 9. Typical load-displacement curves of r3 and r9 specimens (Here, the stress is used as the longitudinal axes to reduce the influence of thickness) Obviously, r9 specimens obtained higher crushing stress during the crushing process as compared with r3 specimens under the same braiding angle i.e. same braiding structure.

specimen	Cross section (mm²)	Es (kJ/kg)
r3-45	300	78.4
r9-45	301	92.6
r3-18	325	96.6
r9-18	304	106.3
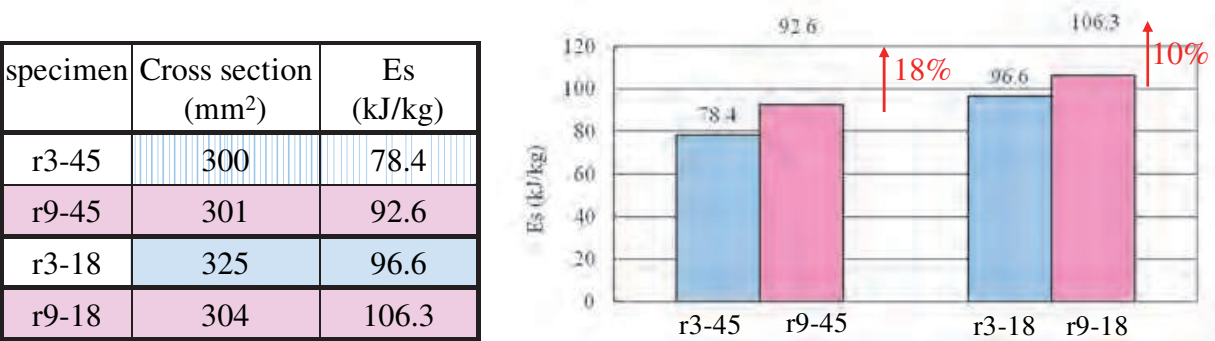
Fig. 10. Comparison of specific energy absorption between r3 and r9 specimens

As illustrated in Fig. 11, with the design of the corner, the geometry of the FRP tubes changed. Here, according to the fracture fashion the FRP tubes, the tube was separated into 8 parts consisting of 2 pieces of long flat walls, 2 pieces of short flat walls and 4 pieces of corners. The *I* of each part ($I_{\text{long flat wall}}$, $I_{\text{short flat wall}}$ and I_{corner}) was calculated separately to get a total *I* of the FRP tube i.e. I_{total}.

$$I_{total} = 4(I_{flat\ wall} + I_{corner}) = 2(I_{\text{long flat wall}} + I_{\text{short flat wall}}) + 4(I_{corner}) \tag{9}$$

Here, $I_{\text{long flat wall}}$, $I_{\text{short flat wall}}$ and I_{corner} are I_{zc} of the long flat wall, short flat wall and corner respectively calculated based on formulas (4~7). For corner part, *r* (inner radius of corner) is considered as 3mm or 9mm according to the used metal mandrel's shape. In this case, while *R* (outside radius of corner) is measured from each specimen, because it is found that the thickness of long flat wall is different with that of short flat wall as shown in Table

1. The length (w) of long flat wall or short flat wall in r3 group tubes is 36-(2x3) i.e. 30 or 24-2x3 i.e. 18. Similarly, w of long flat wall or short flat wall in r9 group specimens is 18 or 6 accordingly.

The detailed calculation results are summarized in the table in Fig.11. For r9 specimens, all of $I_{flat\ wall}$ were decreased a little with an amount of 5.32 mm^4 overall as compare to the r3 specimens. However, the increase of I_{corner} (144.12 mm^4) was too much than the decease part of flat wall region in r9 specimen. Therefore, I_{total} of r9 specimen is much higher than that of r3 specimen. According to formula (3), high I means high U_{bend}. It is considered that the increased U_{bend} contributed to the total absorbed energy directly or indirectly which led to a higher Es in r9 speicmens.

		$I_{\text{Long flat wall}}$	$I_{\text{Short flat wall}}$	I_{Corner}	I_{total}
r3	Outer	4.32	2.59	2.51	43.08
	Inner	4.32	2.59	1.35	
r9	Outer	3.22	1.03	23.38	176.56
	Inner	3.22	1.03	16.51	
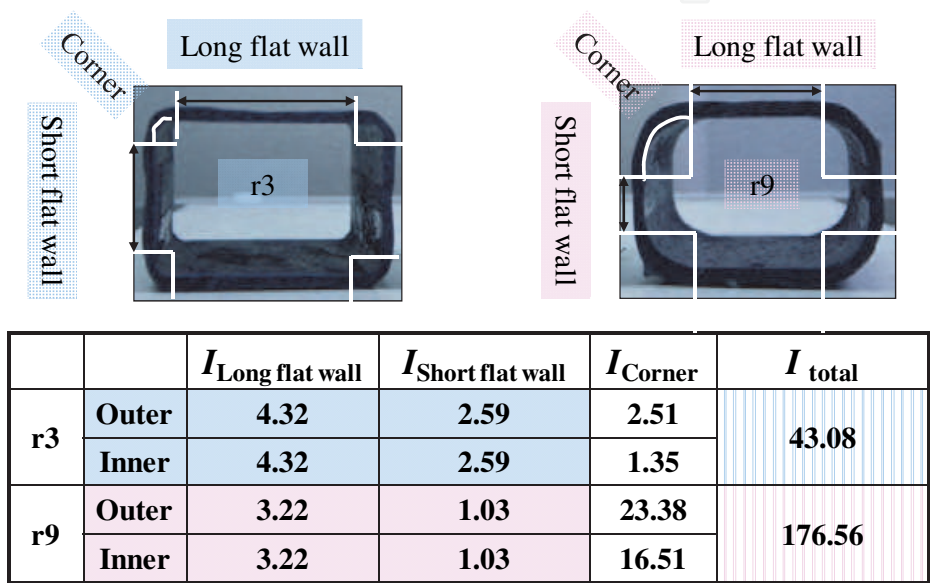
Fig. 11. Parameter about the geometry of each part of R3 and R9 specimens.

4. The combining of both circular and square

4.1 Materials and experiments

The mandrel was designed into three parts (Fig. 12a) i.e. pure circular tube part, cone part and general square tube parts. The beginning circular tube part is for high-efficient energy absorption capability. The end square tube part is to conveniently assemble with other components in assembling process in the automobile manufacture. And a gradual cone part as a joint part between circular and square parts. The mandrel is approximate 400mm long, in which the circular tube part is about 250mm long, the cone part is about 25mm and the square tube is about 125mm. The diameter of circular tube part and the side length of the square tube part are 50mm. On the corners of the square tube part, there is a radius of 9mm. In addition, in order to combine the circular and square parts smoothly, there are some modifications on the cone part. That is to say the cone part is not with a cure cone shape. Here, the study at present is concentrated in both circular and square tube parts only.

Concerning about the fabrication process of preforms, firstly, 48 braiding yarn and 24 middle-end-fibers of Carbon fibers as reinforcement material were used to fabricate braided preforms on the above new designed mandrel by a braiding machine (Murata machinery,
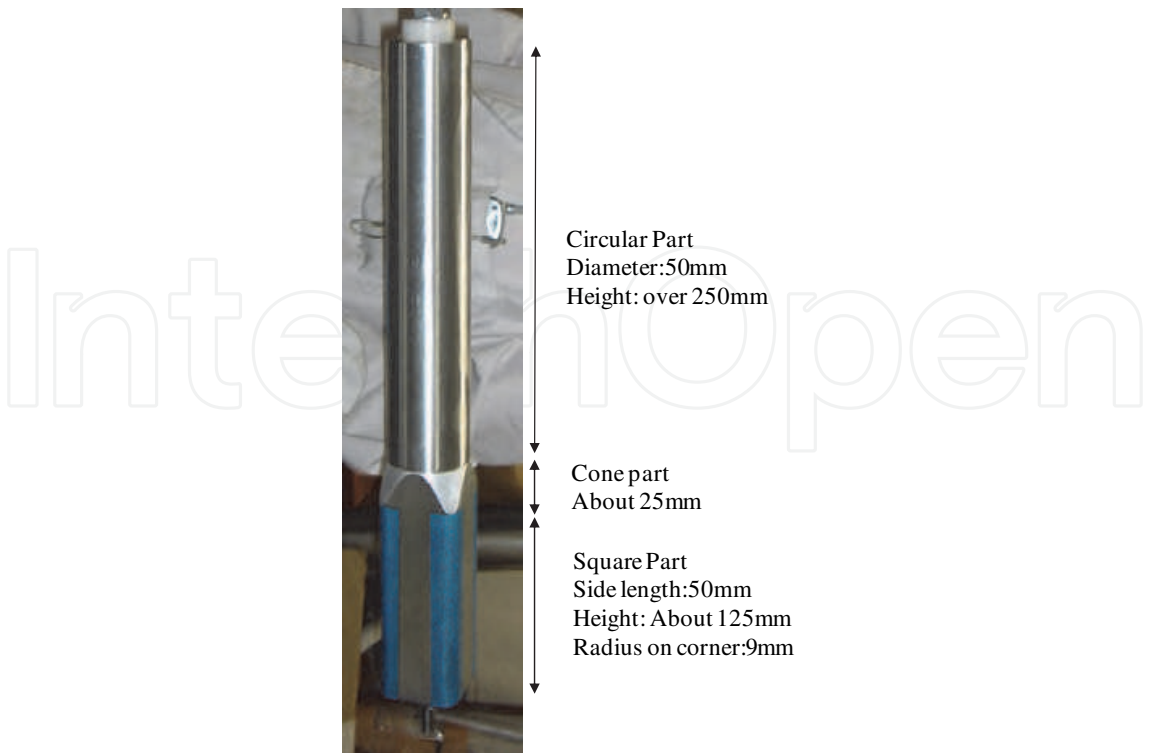
Ltd). With different braiding architecture, three kinds of prefoms (Type 15-15; Type 15-60 and Type 60-60) are made. The former and later numbers represent the braiding angles in the circular part and square part respectively. In details, in Type 15-15 and Type 60-60, the braiding angles are the same in each parts of the tube, i.e. 15 degree or 60, was applied in the whole tube. However, In Type15-60, 15 degree of braiding angle was applied in the circular tube part firstly. When going to the cone area, decrease the moving speed of both bundle and pultrusion of fabricated braids to fabricate the braids with a 60 degree braiding angle in square tube parts. Those fabricated carbon fiber braided preforms i.e. Type 15-15; Type 15-60 and Type 60-60 are compared in Fig. 12b to show the difference of braided structure in circular and square parts. Such braiding process was repeated 4 times to accumulate 4 layers in order to get a suitable thickness of braids. Then, a skin braided layer mentioned in the above sections was fabricated on the most-outside of all of preforms in order to retain the shape during the impregnation process. Finally, the preforms were impregnated with Epoxy resin (XNR 6805 from Nagase ChemteX Corporation) by VARTM and were cured in an oven at 80°C for 10 hours.

The braided composites were drawn out from the mandrel and cut into approximate 300mm long specimens as shown in Fig.13. Similar to the mandrel shape, the specimens have 200mm in circular tube part; 25mm in cone part, and 75mm in square tube part. The specifications of the specimens are given in Table 2. Because the change of the shape, the geometry and area of cross section is changed from the circular tube part, cone tube part to square tube part. Apart from the shape's change, the density also changed because of the change of braiding architecture. Therefore, one piece of the circular tube part and square tube part were segmented to measure the weight and thickness in order to get the density of both parts in each specimen. The fiber volume fraction of all specimens was about 50%. Additionally, a 45° taper was chamfered at top end of the circular tube part of each specimen before compression axially in order to initiate progressive crushing.
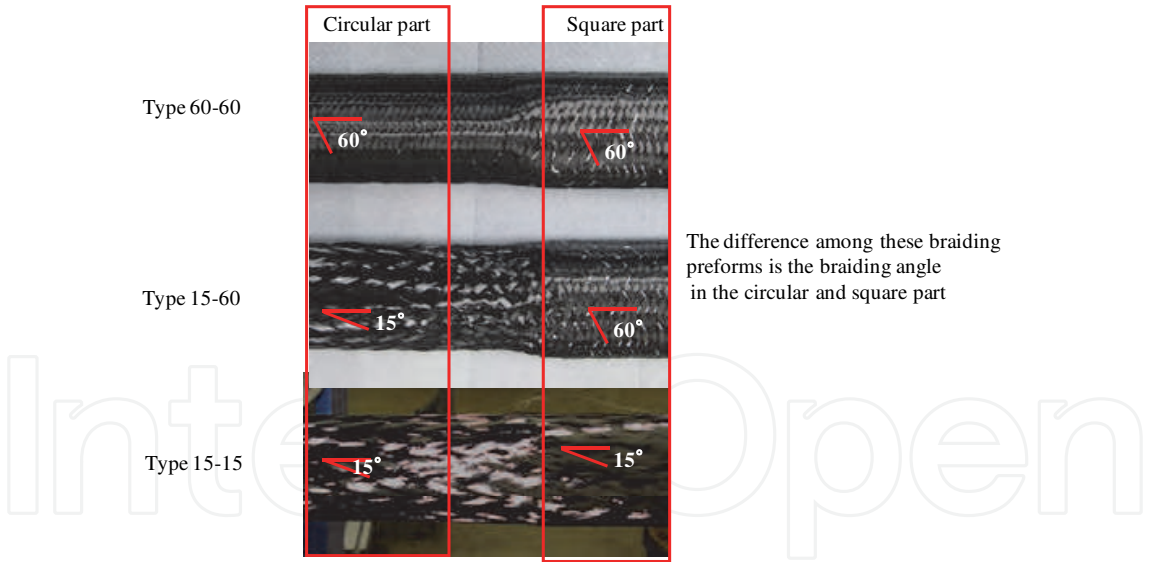
An INSTRON 4206 universal testing machine with the maximum load cell of 100kN was employed in quasi-static compressions. The composite tubes were crushed between parallel steel flat platens from the circular tube part at a constant speed of 50mm/min. A 50points/second data sampling rate was chosen to record the track of the load during the whole crushing process.

4.2 Results and discussion

For Type 15-15, the braided FRP specimen was crushed in a splaying mode as an example shown in Fig. 14. The crushed tube wall was split into pieces and bent towards both inside and outside of the tube like a splaying flower during the whole crushing process. From the load-displacement curve of Type 15-15 shown in Fig.14, it could be said that the braided composite tube was crushed in progressive crushing because their crushing load fluctuated with a small oscillation particularly in circular tube part. However during the crushing process through the cone and square tube parts, the load drops twice from 85kN to 50kN. On the other hand, for Type 15-60 (Fig. 15), crushing fashion is similar to the former one, i.e. many splitting are formed and bend to both sides of the tube wall. The different crushing performance between Type 15-15 and Type 15-60 is concentrated in the period during crushing of the cone part and square tube part. It is obvious that the load curve of Type 15 has dropped twice (from 85kN to 50kN) while it did not occur in Type 15-60. On the contrary, the load of Type 15-60 show an increase trend during the crushing period from cone tube part to square tube part. For Type 60-60, there is quite different crushing

Circular Part
Diameter:50mm
Height: over 250mm

Cone part
About 25mm

Square Part
Side length:50mm
Height: About 125mm
Radius on corner:9mm

(a)mandrel

(b) Carbon fiber braided performs

Fig. 12. (a) a mental mandrel with a novel three-phases geometry: circular part of 250mm, cone part of 25mm and square part of 125mm; (b) Carbon fiber braided performs of Type 15-15; Type 15-60 and Type 60-60 showing the difference in braided angle between circular part and square part.

performance. When the compression commences, fracture initiates from the taper region. Then the tube wall was crushed into many fragments which is different with the splitting fronds in the above two specimens. When the tube was compressed to the displacement of

50mm, it can be clearly observed that buckling fracture generated under these fragments (Fig. 16 (a)). When the tube was compressed to the placement of 100mm, serious buckling fractures occurred in the cone tube part (Fig.16(b)) and the load decreased rapidly. It is considered that the specimen of 60-60 did not fracture in a stable progressive crushing mode.

Fig. 13. Fabricated carbon braided FRP tubes with a novel three-phases geometry: circular part of 200mm, cone part of 25mm and square part of 75mm

	Circular tube part			Square tube part			Weight of the whole specimen (g)	Height of the whole specimen (mm)
	Thickness (mm)	Cross section (mm²)	Density (g/cm³)	Thickness (mm)	Cross section (mm²)	Density (g/cm³)		
Type 15-15	2.55	420.8	1.51	2.24	429.2	1.51	179.6	300.5
Type 15-60	2.56	421.7	1.50	2.87	555.5	1.57	204.6	300
Type 60-60	3.52	587.6	1.57	2.92	570.5	1.57	259.4	299

Table 2. Specification of specimens (carbon braided FRP tubes with novel three-phases geometry)

In this case, specific energy absorption i.e. *Es* was calculated from the mean crushing load according to the below simplified calculation formula (10)

$$specific\ energy\ absorption\ (Es) = \frac{W}{A \cdot s \cdot \rho} \approx \frac{\overline{P} \cdot s'}{A \cdot s \cdot \rho} = \frac{\overline{P}}{A \cdot \rho} \tag{10}$$

Where, *W* is the work done i.e. the total absorbed energy, *A* is the transverse cross sectional area of the tube, *s* is the crush displacement, ρ is the density of the material, and $\overline{P}$ is the average load during progressive crushing, *s'* is the approximate crushing displacement *s* which ignore the displacement during the initial crushing period.

For Type 15-15 and Type 15-60 which had progressive crushing performance, their *Es* values of both circular and square tube parts based on formula (10) were calculated and list in Table 3. (As mentioned before, the study at present is concentrated on both circular and square parts. Additionally in this new designed geometry, the cone part is not a strict cone in mathematics. In order to simplify discussion, the discussion on cone region is omitted.) Compared to Type15-15, the mean crushing load and *Es* of Type 15-60 in the circular tube

part did not show difference, i.e. the energy absorption capability of Type 15-15 and Type 15-60 are similar in the circular tube part. However, referring to the square tube part, in Type 15-60, the load kept almost stable during the whole crushing process from circular tube part to cone and square tube part in Type 15-60. While there were two load-downs from 85kN to 50kN in Type 15-15. Additionally, the decrease of square tube part compared to the circular tube part in Type 15-15 is 18% while that is 13% in Type 15-60. Therefore, braided FRP with the specific transversal geometry can be enhanced with appropriate braiding texture design. It is considered that with a big braiding angle of 60 degree in the cone part, the main fiber orientation is close to circumference. Axial fibers can sustain the axial compressive load effectively but hard to prevent propagation of the longitudinal central crack. On the contrary, circumferential fiber can prevent the spreading out of the axial fibers until shearing fractures occur. Thus, when crushing the cone part and square tube part, cracks seemed controlled in a way in Type 15-60 which resulted in no apparent drop of the load and higher energy management consequently.
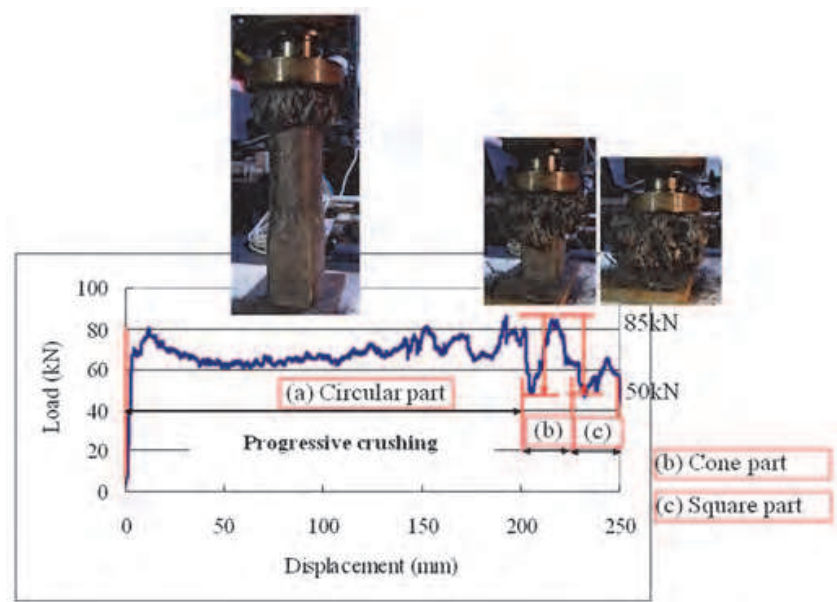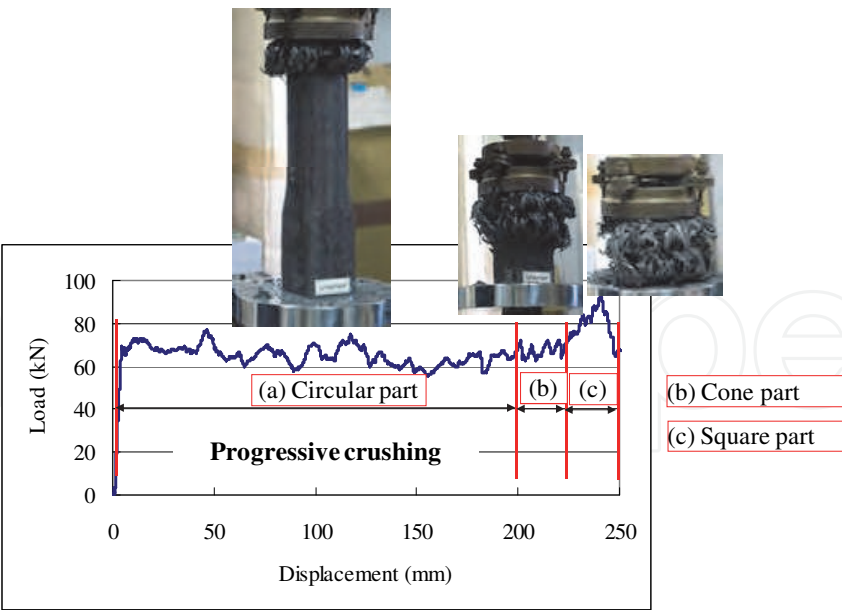

Fig. 14. The load-displacement curve and crushing fashion of Type15-15 during the crushing process (a) circular tube part; (b) cone tube part; (c) square tube part.

	Type 15-15		Type 15-60	
	Circular	Square	Circular	Square
A (mm^2)	420.8	429.2	421.7	555.5
ρ (g/cm^3)	1.51	1.51	1.50	1.56
$\overline{P}$ (kN)	68.59	57.42	67.22	79.69
Es (kJ/kg)	107.9	88.6	106.3	92.0

Table 3. Parameters and energy absorption capability of the specimens carbon braided FRP tubes with novel three-phases geometry

Fig. 15. The load-displacement curve and crushing fashion of Type15-60 during the crushing process (a) circular tube part; (b) cone tube part; (c) square tube part.
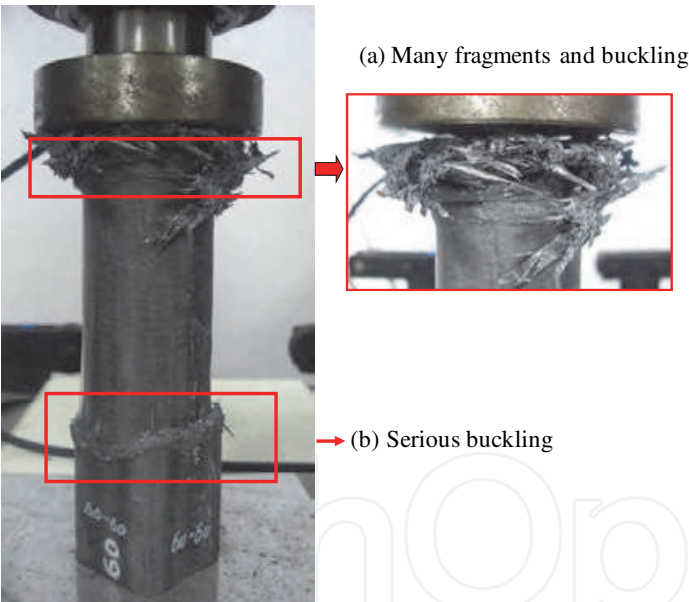

Fig. 16. The crushing fashion of Type 60-60 during the crushing process (a) buckling on the top of the circular tube part; (b) serious buckling in cone tube part.

5. FRP tubes compressed under designed devices

5.1 Materials and experiments
5.1.1 FRP tube with circular transversal cross section
Prepreg yarn consisting of epoxy resin and carbon fiber bundles made of 12,000 filaments with a diameter of 6.8μm was used to fabricate FRP tube with circular transversal cross section by braiding technology. The fabrication process of braiding structure is listed as followings:

1. Initially, 48 bundles of prepreg yarn as braiding yarns were fabricated on a circular metallic mandrel with a braiding angle of 60°. (As illustrated in Fig.17 (a), braiding angle is the angle between the braiding yarn and axial direction.)

(a) Schematic illustration of
a circular braided structure

(b) Photograph of a circular
braided carbon/Epoxy tube
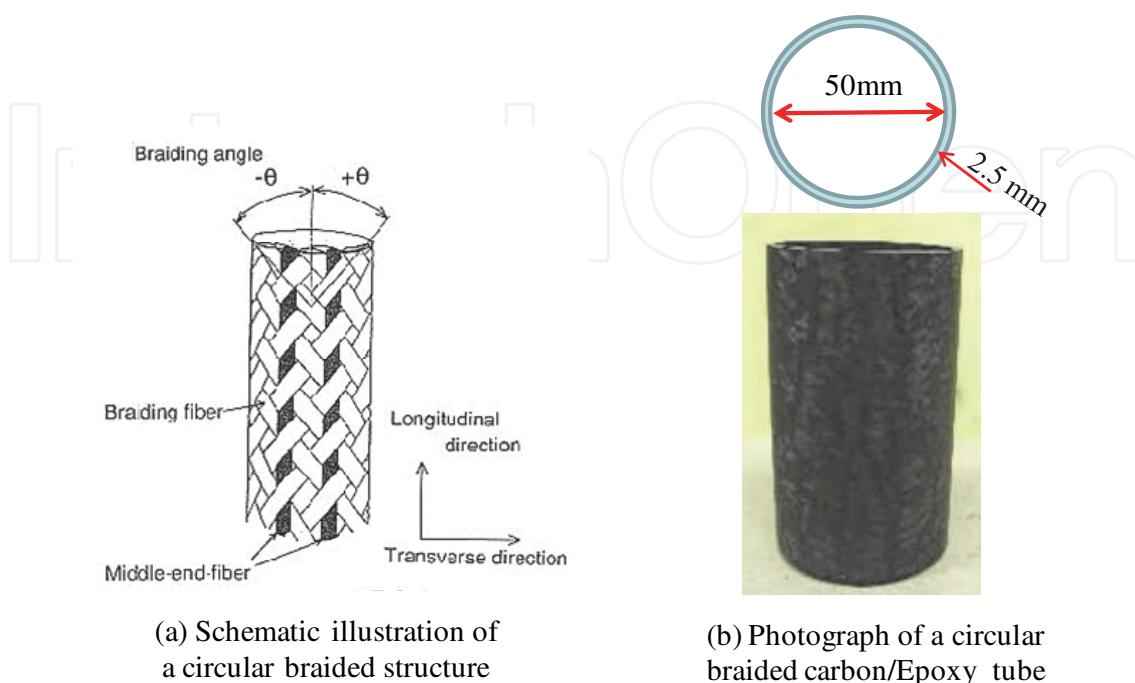
Fig. 17. Braided carbon/Epoxy circular composite tube with an inner diameter of 50mm and a thickness of 2.5mm.

2. Secondly, 48 braiding yarns and 24 middle-end-fibers were used to fabricate the 2nd to 5th layers with a braiding angle of 15°. (Here, middle-end-fiber is the yarn located paralleled to the axial direction while braiding yarn are alternately cross over middle-end-fibers with an angle of 15.)
3. Then the 6th layer with a same fiber architecture as the 1st one was fabricated in the outermost layer. The 1st and 6th layers are the skin layers of braiding preform in order to get a smooth surface during curing process.
4. After braiding fabrication, shrink tape was wrapped on the surface of the braided preforms under an appropriate pressure to get a high fiber volume fraction and low void fraction. After that, it was cured in an oven at a constant temperature of 130°C for 4 hours. (The temperature was increased from room temperature to 130°C with a rate of 5°C/min)
5. Finally, after the shrink tape was removed, the composite pipes (Fig.17(b)) were drawn out from the mandrels. The fabricated braided carbon/epoxy composite pipes were with a fiber volume fraction of about 52% and a thickness of 2.5mm, an inner diameter of 50mm.

In order to assess the viability of these new kinds of collapse triggers, the Fig. 6 devices were compared against the taper trigger which is the most common trigger involved FRP tubes. According to the collapse trigger, the segmented circular tubes with a height of 50mm are divided into two groups. Taper group, was composed of the braided carbon/Epoxy circular tubes of Taper-15, Taper-45 and Taper-75. The flat end of one side of those specimens were chamfered to sharp edge in 15°, 45° or 75°. For the Device group tubes, there was not any

modification on their ends. However, the afore explained devices are capped onto the FRP tubes before compression test. Depending on the device type, the specimens were named. For example, the braided carbon/Epoxy circular tube, which was capped C-Inner 3 type device, was called Inner-3. In the same way, Inner-5, Outer-3 and Outer-5 were named correspondingly.

5.1.2 FRP tube with square transversal cross section

Two kind of FRP tubes with a similar square transversal cross section were employed to investigated the energy absorbing mechanism under the effect of S-Inner 2 device in both quasi-static and dynamic compression condition. One is Carbon UD tube which has unidirectional carbon fiber as reinforcement and polyester as matrix. The other is Carbon MWK tube which is involved carbon multi-axial warp knitted (MWK) fabric. The laminate lay-ups of Carbon MWK tube consists of glass sward mat (Glass SM, 360g/m²), carbon MWK fabric (600g/m²), glass roving (Glass UD, 4450 g/Km), and another carbon MWK layer (600g/m²) from outside to inside in the thickness. Here, in the MWK carbon fabric in both FRP tubes, two unidirectional carbon fiber layers i.e. 90º/0º were combined by knitted yarn. Both of the square FRP tubes are fabricated by pultrusion process. Unidirectional fiber bundles or MWK fabrics are drawn together through the resin rain. Then the resin coated fibers are drawn through specific heated die where the fibers are impregnated with resin and cured to have a desirable geometry similar to the die. After cooled, the FRP tubes are cut into pieces in any ordered length.

The introduction about square FRP specimens is given in Table 4 as well as their photographs. Referring to the square geometry in transversal cross section, the FRP tubes have an outside length of 50mm and a thickness of 4.2mm in the flat wall. In particular, there are the internal corners with a radius of 6 mm and external radius of 2mm respectively. Specimens were prepared in 100mm length for quasi-static and 300mm for impact tests. Similarly to the circular FRP tubes, the energy absorption capabilities of square FRP tubes are compared under both S-Inner 2 device and taper triggers with an angle of 45º.
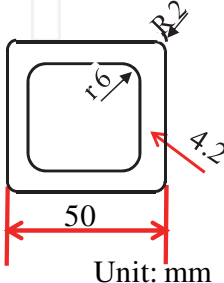
FRP tubes	Photos	Reinforce-ment	Matrix	Reinforcement form	Geometry of transversal cross section	Transversal Cross section (mm²)
Carbon UD		Carbon fibers	Polyester	Unidirectional		769
Carbon MWK		Carbon/glass fibers (Hybrid)	Polyester	MWK and Unidirectional		769

Table 4. Specifications and photographs of the FRP specimens with square transversal cross section

5.1.3 Experiments

Quasi-static compression tests were performed on an INSTRON (4206) universal testing machine at a constant crosshead speed of 5.0mm/min for both circular and square FRP tubes. The test started when the flat compression plate of the machine slightly touched the taper of FRP tube or the device which was capped on one end of the tube. During the compression procedure, five data points every second were recorded to follow the track of the load. Later, three replicate tests were conducted to verify the stability of the energy absorption capability.

On the other hand, impact tests were carried out commercially (in Tokai Techno-research Company) for square FRP tubes additionally. An example of Carbon UD specimen with the usage of S-Inner 2 device as collapse trigger is given in Fig.18 to illustrate the preparation of impact test. After the specimen is fixed on the test machine, the impactor of 120kg which located from 12m height place fall freely to create the impact velocity of 55km/h (15.3 m/s) when it crash the FRP tube. During the impact process, the sampling rate of load is selected 50μs (20 kHz) to obtain a series data of loads. Here something regrettable should be claimed. In case of S-Inner 2 device usage, several duplicate specimens were not done in dynamic compression. The reason will be explain in the following Discussions Section.

5.2 Results
5.2.1 Circular braided carbon/Epoxy FRP tubes

For Taper group tubes i.e. in the cases of taper triggers, the representative load-displacement curves obtained from the axial quasi-static compression tests are shown in Fig.19 (a). The common feature of all of the curves is that the loads increased rapidly in the initial stage, reach a peak value and then dropped slightly. After that, the loads increased again, and finally showed the characteristics of progressive crushing. Although, Taper-15 had the highest peak value at the initial crushing stage and a little different inclination compared Taper-45 and Taper-75, the figures clearly indicate that the Taper group tubes exhibit similar crushing load, in particularly, during the progressive crushing period. However, as shown in Fig.19 (b), the situation is complicated for the Device group tubes. That is, these tubes with different device type displayed distinct mean crush loads. In detailed, the mean crush loads are 82.7kN for Inner-3; 35.8kN for Inner-5; 44.3kN for Outer-3 and 19.2kN for Outer-5. In addition, the mean loads of the tubes capped outer type device were lower than their initial peak values. On the other hand, for the tubes with the inner type trigger, the mean loads were retained at a higher level than the initial peak.

The usage situation of different triggers on the circular braided carbon/Epoxy FRP tubes in quasi-static compression tests are summarized in Table 5. It is found that in the cases of taper trigger, the crushing fashions of the circular FRP tubes are almost the same i.e. the crushed walls were spread out towards both sides of the tube in two-side-bending mode like a spreading flower. However, in the cases of device trigger usage, the fronds show one-side-bending mode. The crush wall was split into pieces and bent inwards by Inner type device or spread outwards by the Outer type device. Those internal fronds seem superposed together tightly whereas, the external fronds are found to be separated. In addition, the *Es* values, calculated from the above Load-displacement curves, is also given in Table 5. Apart from the crushing performance, such closed *Es* values from 86.8 to 94.3 illustrate that the Taper group tubes have the similar energy management. However, quite different *Es* values were obtained with different devices usage. It seems that Inner type device or a small radius associates to higher energy absorption than Outer type device or a big radius. In the usage

of inner type device with a radius of 3mm, the highest value of 110.8 is achieved in C-Inner 3 specimen even compared to that of Taper group tubes.
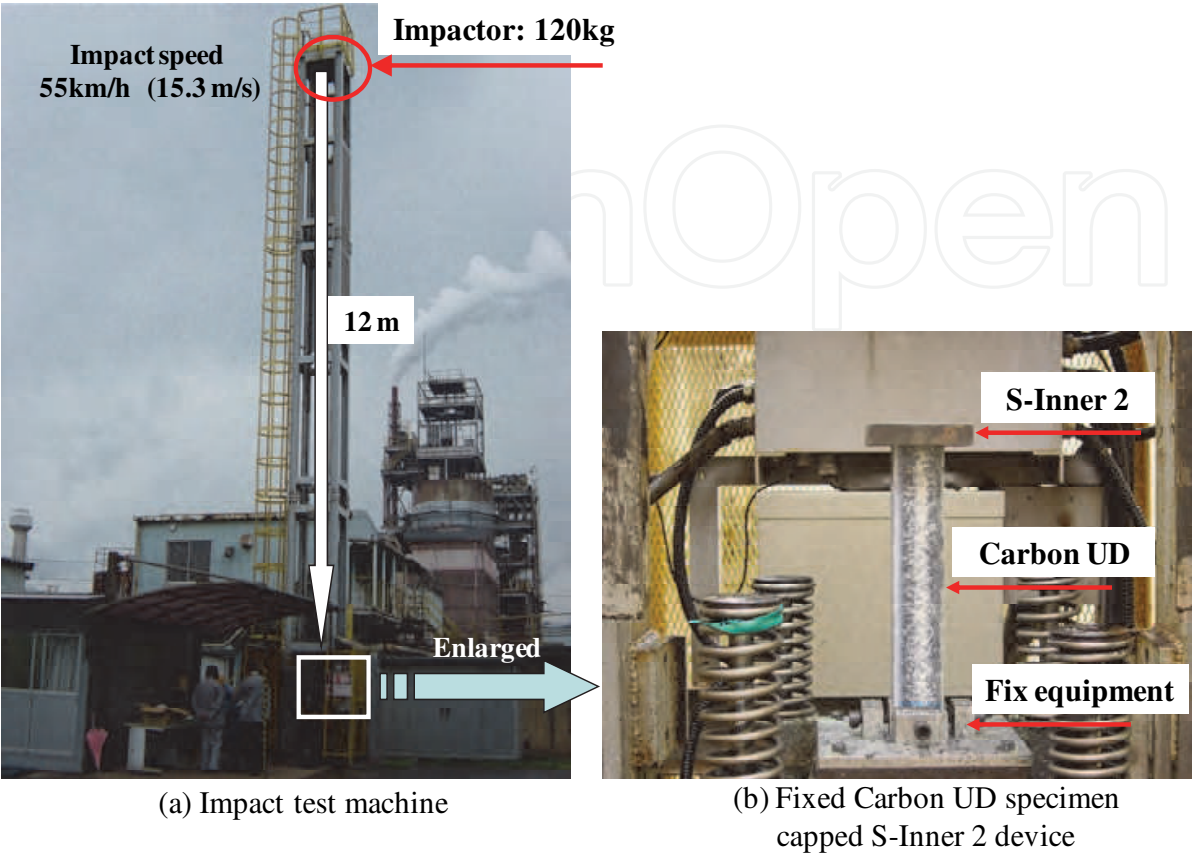

(a) Impact test machine

(b) Fixed Carbon UD specimen capped S-Inner 2 device

Fig. 18. Impact test machine and an example of Carbon UD specimen with the usage of S-Inner 2 device as collapse trigger.
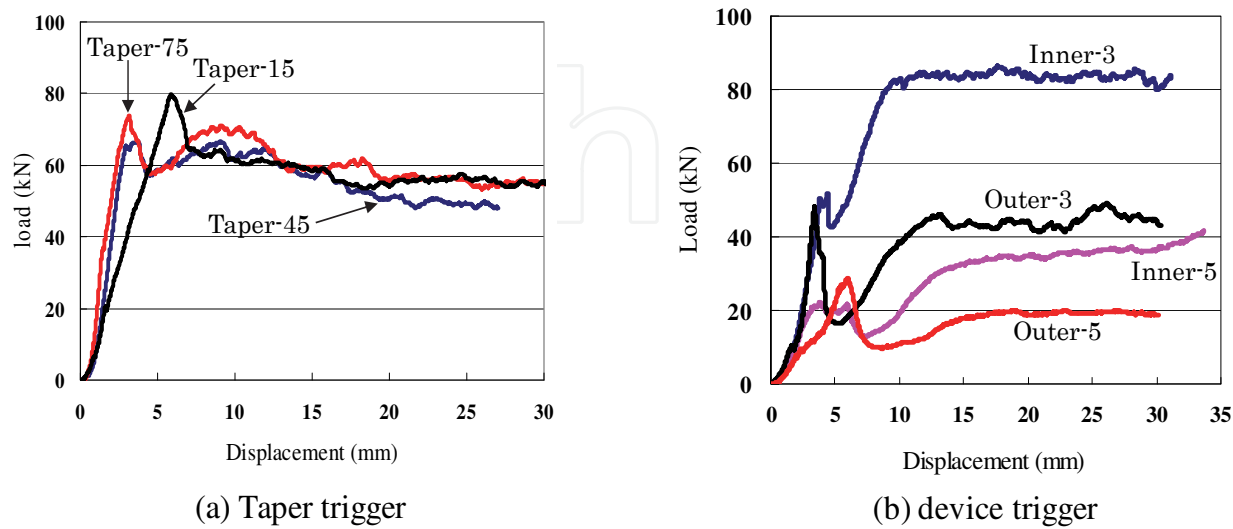

(a) Taper trigger

(b) device trigger

Fig. 19. Typical load-displacement curves of circular braided carbon/Epoxy tubes with different collapse triggers in quasi-static compression tests.
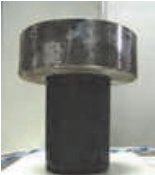
Specimens with their triggers		Specimen	Es (kJ/kg)	After quasi-static compression (Remove the device
Taper (θ:15,45,75)	∠θ	Taper-15	86.8	**(Two-side-bending mode)** External fronds Internal fronds
		Taper-45	94.3	
		Taper-75	87.8	
Device (Inner Type)		Inner-3	110.8	**(One-side-bending mode)** Shoved internal fronds
		Inner-5	43.9	
Device (Outer Type)		Outer-3	58.4	**(One-side-bending mode)** Separated external fronds
		Outer-5	25.4	

Table 5. Fracture performance of circular braided carbon/Epoxy tube with different collapse trigger in quasi-static compression test

5.2.2 Square carbon UD and carbon MWK tubes

The typical Load-displacement curves of Carbon UD and Carbon MWK tubes from both quasi-static and impact tests are shown in Fig.20. The tubes were almost compressed until 50mm in quasi-static compression and more than 150mm in impact test. It is found that no matter which triggers usage, almost the FRP tubes show the progressive crushing performance in both quasi-static and dynamic compression conditions. In particularly, in both quasi-static and impact test, the FRP tubes show the trend that relative higher crushing load can be obtained with the usage of device trigger than that of taper trigger except Carbon UD tube. Carbon UD tube had a relative higher peak load which is over 120kN. After peak value, the load of Carbon UD tube decreased without stopping in dynamic test with the usage of S-inner 2 device and even lower than that of taper trigger after 100mm displacement. That is to say, there is not a satisfied progressive crushing occurred in Carbon UD tube in the condition associated with device and impact. In Fig.21, the photographs of Carbon UD and Carbon MWK tubes with device as collapse trigger in impact tests were compared. As shown in Fig.21(a), the tube wall of Carbon UD was split into many pieces but part of them couldn't be embedded into the inside of the device. That is considered as the main reason why the load got down continuously. On the other hand, as illustrated in Fig.21(b), unlike the former one, the Carbon MWK tube showed a relatively successful crushing performance i.e. almost of the split tube wall were bent into the inside of the device. On the other hand, in the case of the most common collapse trigger i.e. taper, all of the specimens are crushed in two-side-bending mode, i.e. the tube wall was split to many

pieces and bent towards both sides of the tubes. Compared the fronds bending with a small bending curvature in quasi-static test in Fig.22(a/b), the split tube wall sprang back greatly and bending with a relative big bending curvature (Fig.22 (c/d)) in impact test. It is thought that parts of the bending walls did not fracture but still under flexural deformation in impact test.
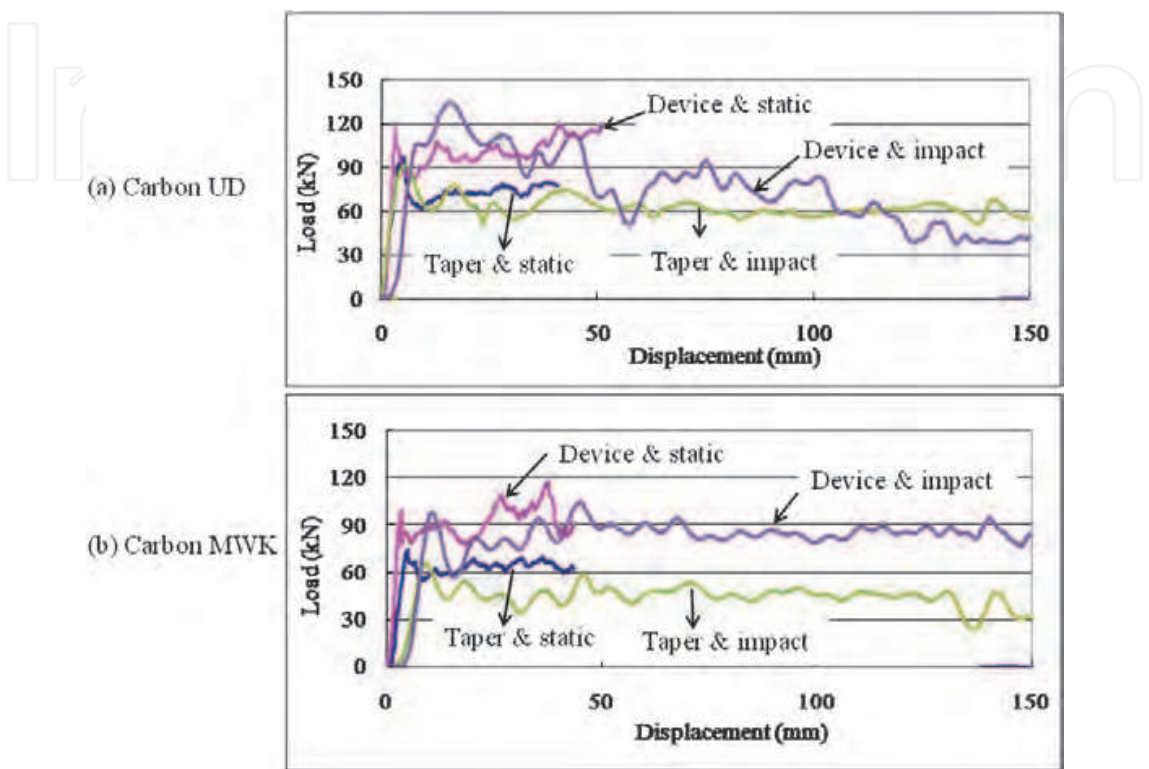

Fig. 20. Typical load-displacement curves of square Carbon UD and Carbon MWK tubes with different collapse triggers in both quasi-static and impact tests.

Their energy managements were discussed based on the *Es* value listed in Table 6. Because that the Carbon UD tube which with the device trigger could not generate progressive

FRP tube	Trigger	Quasi-static	Impact	Impact vs. Static	Inner Device vs. Taper
Carbon UD	45° Taper	55.0	52.1	94.7%(taper)	145.5% (static)
	S-Inner 2 device	80.0	59.6	74.5%(device)	114.4%(impact)
Carbon MWK	45° Taper	47.7	32.2	67.5%(taper)	142.6%(static)
	S-Inner 2 device	68.0	71.3	104.9%(device)	221.4%(impact)

Table 6. Energy management of square FRP tube with different collapse trigger in both quasi-static and impact test.

crushing in impact compression test owing to the decreasing load, *Es* of all the specimens are calculated based on the data from 0 displacement to 150mm in dynamic and 0 to 50mm in quasi-static compression. Additionally, ratios of impact vs. quasi-static test and the one of device vs. taper are calculated to find the lost or increase under the different compression conditions. It is known that *Es* values in dynamic compression test are lower than that in quasi-static compression tests for almost the specimens except Carbon MWK tube with usage of device trigger. For Carbon MWK tubes, there is distinct trend between device and taper trigger. In details, in taper trigger, the *Es* value in dynamic is only 67% of that in quasi-static condition. That is to say, more that 30% is lost in impact test compared the equivalent static values. However, with the usage of device trigger, on the contrary, a similar or a relatively higher *Es* was obtained. From the ratios of Device vs. Taper, it can be concluded that no matter which reinforcement form and compression speed, higher *Es* values can be achieved with the Inner type device trigger usage than that of the taper trigger.
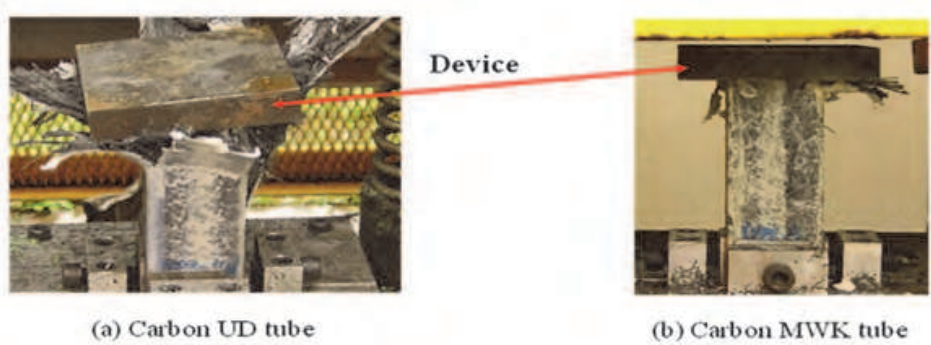

(a) Carbon UD tube (b) Carbon MWK tube

Fig. 21. Photograph of square FRP tubes in impact test with the device as collapse trigger.

(a) Carbon UD after static test (b) Carbon MWK after static test

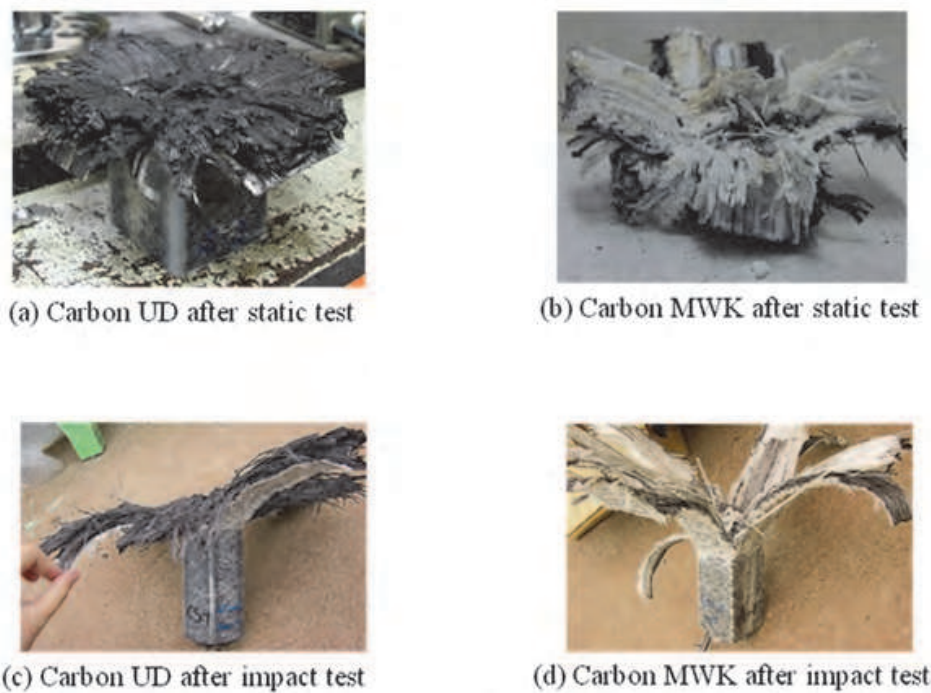(c) Carbon UD after impact test (d) Carbon MWK after impact test

Fig. 22. Photograph of square FRP tubes with taper as trigger after compression test (quasi-static and dynamic)

5.3 Discussions
5.3.1 One-side-bending vs. two-side-bending
From their crushing performances, it is well understood that with the usage of device, the tube wall of FRP is possible to be in One-side-bending mode rather than Two-side-bending in the case of taper trigger. As illustrated in Fig. 5, the tube fronds in One-side-bending mode have a double thick thickness of that in Two-side-bending mode. If the thickness of the tube wall is given, forcing it to be in one-side bending mode would be more effectively in bending behavior. According to the formula (3), the bending energy of fronds is directly affected by *I*. Owing to the double size thickness in one-side-bending mode, section modulus will increase greatly in any kind of shape. For an example, for a piece of flat wall of FRP tube assumed as a beam with a rectangular transversal cross section of (length *w* X thickness *t*), the bending energy can be expressed used formula 11.

$$U_{bend} = \frac{5E \cdot I_{flatwall} \cdot s}{2l^3} = \frac{5E \cdot s \cdot \frac{1}{12} wt^3}{2l^3} \tag{11}$$

Here, *E*, *I*, *s* and *l* are the modulus, inertia moment, compression displacement and the height of the beam. In one-side-bending mode, the section modulus will increase 8 times because of double *t*. Therefore the total U_{bend} i.e. the whole bending energy of all of the fronds would increases 4 times. It is considered that the increase U_{bend} contributes to the enhanced energy absorption capability indirectly. On the other hand, the most important effect is that with the increased thickness, the bending stresses are increased correspondingly according to the formula (8) and affect the fractures of fiber as well as resin directly. In details, during the bending process, the fronds experience high tensile stresses on the up layers and compressive stresses on the bottom layers. When the stresses exceed the strength of fiber, many fibers fractured.

To clarify the energy absorbing mechanisms, micro-observations were carried out furthermore. The specimens after compression tests were immerged into the polyester resin and then cured in order to maintain the fracture morphology. After that, cured specimens were cut along the axial direction by the diamond cutter and some appropriated axial cross sections through the crush zone were selected and polished for observation on a metallic microscope (reflection type). Here the difficulty of digging the tested specimens from the S-Inner 2 in the case of Inner type device usage in particular after impact test should be mentioned. During the compression process, the FRP tube had expanded and clung to the device. Additionally, the bending fronds compacted tightly in the concave part of Inner type device. As a result, the specimens after compression were very difficult to be taken out from the Inner type device even with a hammer. To hit the FRP tube with a big strength had been avoided, because the morphology of fractures might be damaged. Appropriated strength was applied to the hammer to hit the FRP tube walls carefully and alternately. In some cases, however, such specimens which did not be controlled successfully by the inner type device after impact test had to be destroyed. Those fragments which are filled in the concave part of the Inner type device in an extreme compacted situation were solved by acetone so that the Inner type device could be released for the next experiments. That is the reason why several repeat impact tests couldn't be implemented within the limited stipulated time.

Here the observation results on the flat wall of Carbon MWK composite specimens after impact test were illustrated in Fig. 23 (taper trigger) &24 (device trigger) as examples to compare the effect of triggers on the energy absorbing mechanisms of FRP tubes. In the case of taper trigger, as shown in Fig.23, two-side-bending behaviors could be seen. Although some fiber fractures could be found in the inside bending fronds, many intro/inter delaminations generated in the middle and outside fronds instead. Additionally, a big distance could be found between middle and outside layers after the compression was released. It is considered that the middle fronds sprung back because of the lack of fiber fractures. On the other hand, as illustrated in Fig.24, the flat wall of carbon MWK tube shows these features: bending of tube walls towards inside only; many inter and intro-delaminations in the middle layers; many transversal cracks and fiber fractures in both surfaces layers. Here, an attention should be paid that although many inter or intro delaminations occurred, those independent fronds did not separated each other even after it was released from the control of device. They touch and bent in a similar bending curvature towards inside.
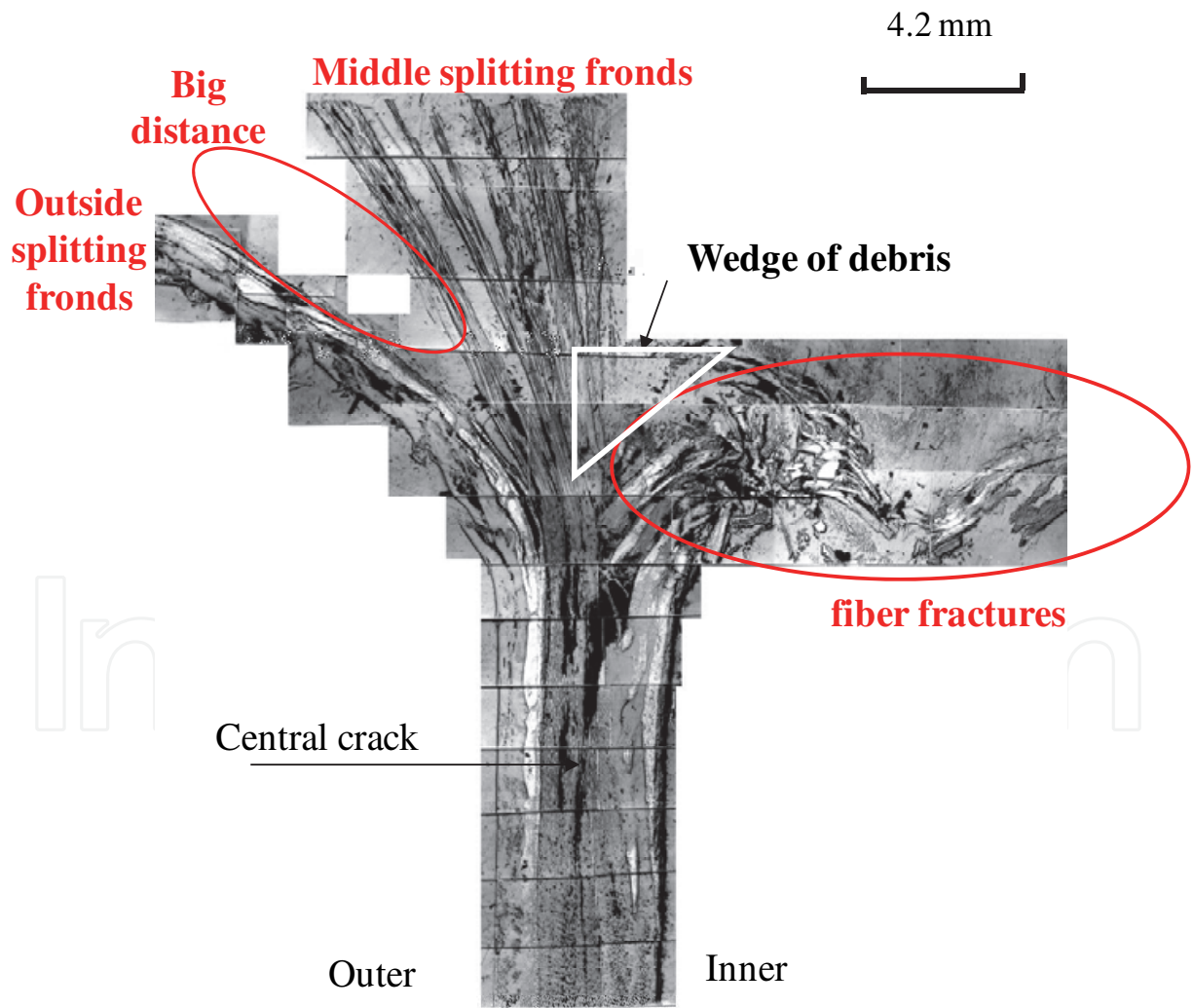

Fig. 23. Observation of flat wall of Carbon MWK tube after impact test illustrating two-side-bending behavior, many splitting frond and some fiber fractures (taper trigger)
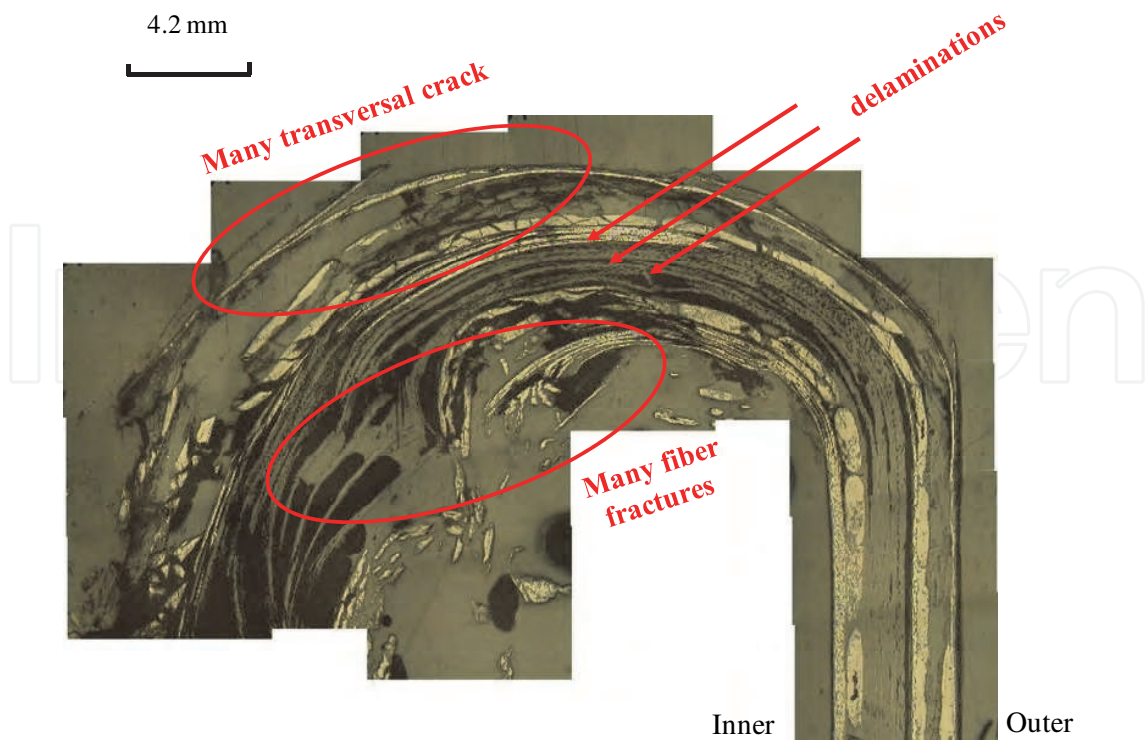
Fig. 24. Observation of flat wall of Carbon MWK tube after impact test illustrating that the fronds were being bent towards inside only and many fracture generated (S-Inner 2 device trigger).

5.3.2 Effects of the radius (*R'*) and the type of device

From the quasi-static compression experimental results of the braided carbon circular tubes, it can be said that devices can trigger progressive crushing similar to taper. However, unlike taper, device can also change the energy absorption capacity of the FRP tubes significantly. Inner type could be said to be better than outer type and a smaller R' confers better energy absorption capability.

Here Inner-3 and Inner-5 specimens were compared their energy absorbing mechanisms in Fig.25. The observation focused on the axial cross section through the crush zone where had been under the R' region of the devices. The common characteristic of both specimens is that the tube walls were delaminated into several layers and bends were towards inside. It is considered that at the beginning of the crushing process, with the limitation imposed by device, the tube wall was forced to bend inwards only. Shearing stresses are induced to split the integrated tube wall into pieces. Braiding confers the characteristic that fibers are oriented continuously. Intra-laminar cracks are therefore difficult to grow. On the other hand, the bonding of each braided fabric layer is relatively weaker, so with the advancement of the crushing platen, inter-laminar cracks (delaminations) occurred and were propagated. However, the propagation of delaminations are different, which is deep in Inner-5 while seemed restrained in Inner-3. Additionally, compared Inner-5, Inner-3 had a relatively smaller radius of bending curvature. During the process of bending the pieces of tube wall over a sharp radius of curvature, it is considered that the radius of curvature (r') is controlled by the radius (R') of the device. Therefore, fronds of Inner-3 experienced relative higher tensile stresses on the convex side and compressive stresses on the concave side.

Subsequently, fibers together with resin would be broken and contributed to higher energy absorption capability.

For a given tube compressed under Inner or Outer types devices with same R', quite different energy managements were found. According to the formulae of (3) and (8), they should have similar bending energy and bending stresses. However, obviously Inner type device show greater contribution to energy absorption of FRP tubes. Here the fracture space is considered as the major factor. When the tube wall has to be bent inwards or outwards, the fracture space will be shortened in the case of Inner type or expanded in that case of Outer type device. After the tube wall shears or splits into pieces of "independent" fronds, in the case of inner type device, these "independent" fronds have to be superposed each other owing to the shortened fracture space and shoved the adjacent ones below it with the advancement of the compression process, whereas that will not occur in the case of outer type device because those fronds are separated in an extended fracture space. When the adjacent fronds shove each other, they touch tightly and slide in order to get a space and bend through almost the same bending curvature during the whole compression process, which will cause frictional stresses on the touched surfaces between any two adjacent fronds. Frictional stresses action on the surface of fronds, break fiber as well as resin or generate heat energy at some degree. Apparently, this kind of friction generated by inner type device contributes to the total absorbed energy greatly. Fairfull and Hull [39] had investigated the energy absorbed by the frictional processes in the axially crushing of glass cloth/epoxy tubes. They claimed that frictional energy could account for more than 50% of the total energy absorbed. If the influences of bending curvatures of fronds are ignored temporarily, it could be inferred that the inner type device is better than taper trigger, and taper trigger is better than outer type device, because the friction effect from taper trigger is considered a blend of half from the inner type device and half from the outer type device.
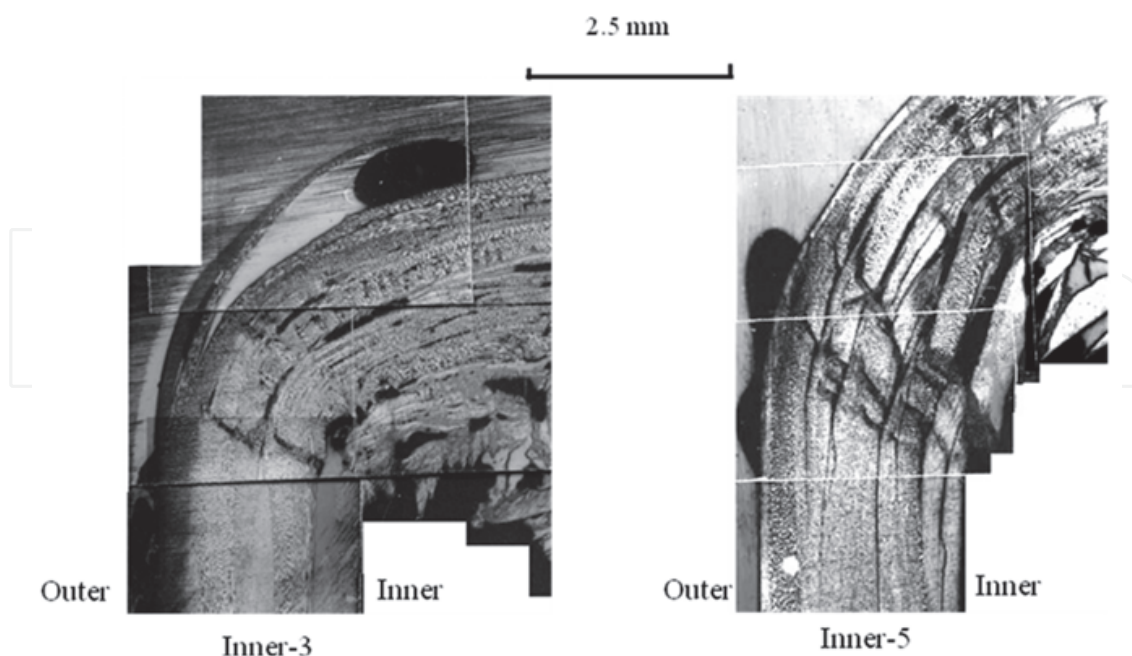

Fig. 25. Observation on the cross sections of Inner-3 & Inner-5 specimens (the crush zone which had been under the R region of device illustrates the different radii of bending curvatures and the propagation of delaminations.)

6. Conclusions

FRP tubes have a very complicated energy absorption mechanism during progressive crushing process. It is considered that the energy absorbed by fiber fracture can contribute to the total absorbed energy significantly. Therefore, an attempt of design of fiber fractures was carried out in current study with an attempt to apply the FRP tubes as energy absorption component in a vehicle.

Crushing behavior of FRP tube was considered related in appearance of the bending behavior of beam. Here mechanism model of a bending beam was used to simulate the bending fronds of FRP tube. It is found that the bending energy is in direct proportion of I, i.e. the moments of inertia of the section area which is determined by the geometry. Therefore two improvement methods based on design of the bending energy through the geometry design were proposed. In method of mimic square to circular, two types of mandrels (r3 and r9 mandrels) with 3mm or 9mm radius modification on the corners were employed to determine the effect of design of the geometry. It is found that Es of the CFRP tubes fabricated on the r9 mandrel were improved significantly as compared to that fabricated on the r3 mandrel even with the same fiber architecture and similar size of cross section area. The influence of the geometry is discussed in terms of I. It is found that trough a reasonable geometry design, the energy absorption management of FRP tube with a bigger I can be improved.

In the method of the combining both circular and square, the CFRP tube with a new geometry, which utilizing both circular cross-section for its higher energy absorption capability and square cross-section for its assembling convenience with other components, was designed. Additionally, braiding texture is used as fiber reinforcement form based on the considerations of cost and preforms fabrication. It was also shown that the braiding texture is helpful to improve the crushing performance of FRP tube with this kind of geometry, particularly during the crushing different cross section process such as from circular tube part to cone part or from cone part to square tube part.

Additionally, a method aims a thicker thickness and a very small bending curvature of bending fronds according to the formula of bending stress. On the other hand, FRP tubes generally need a collapse trigger mechanism to generate stable, progressive, high energy crushing. Therefore, in the study, bending stress was under consideration with collapse trigger mechanism. The target of present experiments is to design a new collapse trigger for the practical application of FRP tubes which is possible to enhance their energy absorption capability.

Four types of devices are designed and used in the axial quasi-static compression tests of braided carbon/epoxy tube with a circular transversal cross section. They include inner and outer types with a radius of 3mm or 5mm. It was found that the devices could trigger progressive crushing similar to taper. However, unlike taper, devices can change the energy absorption capacity of the crushed materials significantly. Inner type device could be said to be better than outer type device because of high friction and a smaller radius confers better energy absorption capability because of high bending stresses.

Additionally an inner type device with a square transverse cross section and $R'2$ was designed for the FRP tube which has a square transversal cross section. The square FRP tubes were compressed in impact test with the usage of device in order to investigate the effect of device under dynamic condition. The results are evaluated in comparison with both taper and equivalent quasi-static values in order to find the effect from the reinforcement

form in the impact test with device. It is found that texture structure (such as multi-axial warp knitted fabric) is better than unidirection in the case of usage of device, because the texture structure can control fiber layers well in bending behavior. Because of the double size thickness in one-side bending, apart from the increased the bending energy, bending stresses are also increased significantly. Many fibers were broken consequently and the fiber fracture energy i.e. U_{ff} increased greatly. As result, the higher energy absorption capability could be obtained.

7. Acknowledgments

8. Appendix

Notation

|	
U_T	total absorbed energy
U_{split}	the energy absorbed by splitting the integrated tube wall into pieces of fronds
U_{cc}	the energy absorbed by the initiation and propagation of the central crack
U_{de}	the energy absorbed by delaminations
U_{bend}	the energy absorbed by the bending of fronds
U_{ff}	the energy absorbed by fiber fracture
U_{fr}	the energy associated with friction
l	height of a beam (frond)
F	an external force
s	The crush displacement along longitudinal i.e. x direction
y_{max}	the maximum distance in y direction
M	the bending moment of the beam (y trial)
x	any point in x direction from 0 to s displacement
E	modulus of the beam (frond)
A	area of cross section
t	thickness
Es	specific energy absorption
I_{corner}	the I_{zc} of the corner region
$I_{flat\ wall}$	the I_{zc} of flat wall
$I_{long\ flat\ wall}$	the I_{zc} of long flat wall
$I_{short\ flat\ wall}$	the I_{zc} of short wall
I_{total}	total I_{zc} of the FRP tube

w	length of flat wall
R	outside radius of the curvatures of the corner
r	inside radius of the curvatures of the corner
W	the work done i.e. the total absorbed energy
ρ	the density of the material
$\overline{P}$	the average load during progressive crushing
s'	the approximate crushing displacement s which ignore the initial displacement
σ	bending stresses
r'	radius of the bending curvature of the frond (beam)
R'	radius of the curvature of the concave or convex part on the device
w	length of flat wall

9. References

[1] Rosen, R.W., Mechanics of composite strengthening. In *Fiber Composite Materials*, American Society for Metals, Metals Park, OH, pp.37-76, 1965.

[2] Thornton, P.H. & Magee, C.L., "The Interplay of Geometric and Materials Variables in Energy Absorption", *Journal of Engineering Materials and Technology*, Vol. 99, pp. 114-120, (1977).

[3] Thornton, P. H. "Energy Absorption in Composite Structures," *Journal of Composite Materials*, Vol. 13, pp. 247-263 (July 1979)

[4] Cronkhite, J.D., Hass, T.J., Berry, V.L. & Winter, R., Investigation of the crash impact characteristics of advance airframe structure. USARLT-TR-79-11, 1979.

[5] Farley, G.L., "Energy Absorption of Composite Materials", *Journal of Composite Materials*, Vol. 17, pp. 267-279, (1983).

[6] Hull, D., "A Unified Approach to Progressive Crushing of Fibre-Reinforced Composite Tubes", *Composites Science & Technology*, Vol. 40, pp. 377-421, (1991).

[7] Thornton, P.H. & Edwards, P.J., "Energy Absorption in Composite Tubes", *Journal of Composite Materials*, Vol. 16, pp. 521-545, (1982).

[8] Farley, G.L. & Jones, R.M., "Crushing Characteristics of Continuous Fiber-ReinforcedComposite Tubes", *Journal of Composite Materials*, Vol. 26, pp. 37-50, (1992).

[9] Farley, G.L., "The Effect of Fiber and Matrix Maximum Strain on the Energy Absorption Capability of Composite Materials", *Journal of Composite Materials*, Vol. 20, pp. 322-334, (1986).

[10] Hamada, H., Coppola, J.C. & Hull, D., "Effect of Surface Treatment on Crushing Behaviour of Glass Cloth / Epoxy Composite Tubes", *Composites*, Vol. 23, No. 2, pp. 93-99, (1992).

[11] Hull, D. & Clyne, T.W., *An Introduction to Composite Materials*, Second Edition, Cambridge University Press, Cambridge, (1996).

[12] Hamada, H., Ramakrishna, S. & Satoh, H., "Crushing Mechanism of Carbon Fibre /PEEK Composite Tubes", *Composites*, Vol. 26, No. 11, pp. 749-755, (1995).

[13] Schmueser, D. & Wickliffe, L.E., "Impact Energy Absorption of Continuous Fibre Composite Tubes", *Journal of Engineering Materials and Technology*, Vol. 109, pp. 72-77, (1987).

[14] Dorey, G., "Impact and Crashworthiness of Composite Structures", *Structural Impact and Crashworthiness*, Ed. Davies, G.A.O., Vol. 1, pp. 155-192, Elsevier Applied Science Publishers, London, (1984).

[15] Tao, W.H., Robertson, R.E. & Thornton, P.H., "Effects of Material Properties and Crush Conditions on the Crush Energy Absorption of Fiber Composite Rods", *Composites Science and Technology*, Vol. 47, pp. 405-418, (1993).

[16] Karbhari, Vistasp M., Falzon, Paul J., and Herzberg, Israel "Energy Absorption Characteristics of Hybrid Braided Composite Tubes," *Journal of Composite Materials*, Vol. 31, No. 12. pp.1165-1186, (1997).

[17] Farley, Gary L and Jones, Robert M. "Crushing Characteristics of Continuous Fiber-Reinforced Composite Tubes," *Journal of Composite Materials*, Vol. 26, No. 1, pp. 37-50 (1992).

[18] Hull, D. "Axial crushing of fiber reinforced composite tubes", In structural crashworthiness, ed. Jones, N. & Wierzibichi, T., Butterworths, London, pp. 118-135, (1983).

[19] Hamada, H., Coppola, J.C., Hull, D., Maekawa, Z, & Sato, H., "Comparison of Energy Absorption of Carbon / Epoxy and Carbon / PEEK Composite Tubes", *Composites*, Vol. 23, No. 4, pp. 245-252, (1992).

[20]. Hamada, H., Ramakrishna, S. & Sato, H., "Effect of Fiber Orientation on the Energy Absorption Capability of Carbon Fiber / PEEK Composite Tubes", *Journal of Composite Materials*, Vol. 30, No. 8, pp. 947-963, (1996).

[21] Schmueser, D. W. and Wickliffe, L. E. "Impact Energy Absorption of the Continuous Fiber Composite Tubes," *Journal of Engineering Materials and Technology*, Vol. 109, pp. 72-77 (January 1987).

[22] Karbhari, Vistasp M. "Progressive Crush of Resin Transfer Molded Square Tube Stiffened Beam Elements," *Journal of Composite Materials*, Vol. 31, No. 10. pp.981-1001 (1997).

[23] Hamada, H., Nakai, A., Kameo, K., and Takeda, N. "Crushing Performance of Braided Composites," *Proceedings of the Eighth Japan-U. S. Conference on Composite Materials,* September 24-25, pp. 467-475 (1998)

[24] Mamalis, A.G., Manolakos, D.E., Viegelahn, G.L., Yap, S.M. & Demosthenous, G.A., "On the Axial Crumpling of Fibre-Reinforced Composite Thin-Walled Conical Shells", *International Journal of Vehicle Design*, Vol. 12, No. 4, pp. 450-467, (1991).

[25] Hamada, H., Ramakrishna, S. & Sato, H., "Effect of Fiber Orientation on the Energy Absorption Capability of Carbon Fiber / PEEK Composite Tubes", *Journal of Composite Materials*, Vol. 30, No. 8, pp. 947-963, (1996).

[26] Farley, G.L. & Jones, R.M., "Crushing Characteristics of Composite Tubes with "Near-Elliptical" Cross Sections", *Journal of Composite Materials*, Vol. 26, No. 12, pp. 1741-1751, (1992).

[27] Kindervater, C.M., "Energy Absorption of Composites as an Aspect of Aircraft Structural Crash-Resistance", *Developments in the Science and Technology of Composite Materials*, Ed.s Fuller, J. *et al.*, pp. 643-651, Elsevier Applied Science Publishers, London, (1990).

[28] Mamalis, A.G., Yuan, Y.B. & Viegelahn, G.L., "Collapse of Thin-Wall Composite Sections Subject to High Speed Axial Loading", *International Journal of Vehicle Design*, Vol. 13, No. 5-6, pp. 564-579, (1992).

[29] Y. Yang, Y. Nishikawa, A. Nakai, U. S. Ishiaku, H. Hamada, "Effect of cross-sectional geometry on the energy absorption capability of unidirectional carbon fiber reinforced composite tubes", *Science and Engineering of Composite Materials.* Vol.15, pp. 249-263, 2008.

[30] FARLEY, G.L., "The Effects of Crushing Speed on the Energy-Absorption Capability of Composite Tubes", *Journal of Composite Materials*, Vol. 25, pp. 1314-1329, (1991).

[31] MAMALIS, A.G., MANOLAKOS, D.E., DEMOSTHENOUS, G.A. & IOANNIDIS, M.B., "Axial Collapse of Thin-Walled Fibreglass Composite Tubular Components at Elevated Strain Rates", *Composites Engineering*, Vol. 4, No. 6, pp. 653-677, (1994).

[32] A.G. Mamalis, D.E. Manolakos, M.B. Ioannidis and D.P. Papapostolou, 'On the response of thin-walled CFRP composite tubular components subjected to static and dynamic axial compressive loading: experimental', *Composite Structures*, Vol.69 pp.407-420, (2005).

[33] D. Hull, 'Energy Absorption of Composite Materials under Crash Conditions', *Proceedings of the Fourth International Conference on Composite Materials (ICCM IV)*, 1982, 1, 861-870.

[34] J. Berry and D. Hull, 'Effect of speed on progressive crushing of epoxy-glass cloth tubes', *Conf. Ser. Inst. Phys*, Vol.70, pp.463-470, (1984).

[35] MAMALIS, A.G., MANOLAKOS, D.E., DEMOSTHENOUS, G.A., IOANNIDIS, M.B., The static and dynamic axial collapse of fibreglass composite automotive frame rails. *Composite Structure*, Vol.34, pp.77-90, (1996).

[36] Sigalas, I., Kumosa, M., and Hull, D., Trigger mechanisms in energy-absorbing glass cloth/epoxy tubes, Composite science and technology, Vol.40, pp.265-287,(1991).

[37] Czaplicki, M.J. et al, Comparison of Bevel and Tulip Triggered Pultruded Tubes for Energy Absorption, Composite Science and Technology, Vol.40, pp.31-46,(1991).

[38] Saito, H. et al, Crushing properties of pultruded glass reinforced square tubes, International Journal of Crashworthiness, Vol. 7, No.1, pp.21-33 (2002).

[39] Fairfull, A.H. and Hull, D., Energy Absorption of Polymer Matrix Composite Structures: Frictional Effects, Structural Failure, Ed.s WIERZBICKI,T. and JONES,N., pp.255-279,(1988).
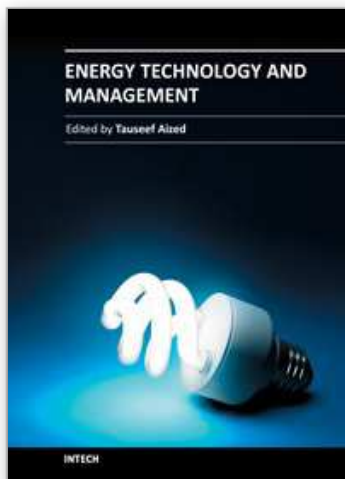
Energy Technology and Management

Edited by Prof. Tauseef Aized

The civilization of present age is predominantly dependent on energy resources and their utilization. Almost every human activity in today's life needs one or other form of energy. As world's energy resources are not unlimited, it is extremely important to use energy efficiently. Both energy related technological issues and policy and planning paradigms are highly needed to effectively exploit and utilize energy resources. This book covers topics, ranging from technology to policy, relevant to efficient energy utilization. Those academic and practitioners who have background knowledge of energy issues can take benefit from this book.

How to reference

In order to correctly reference this scholarly work, feel free to copy and paste the following:

Yuqiu Yang and Hiroyuki Hamada (2011). A Study on Design of Fiber-Reinforced Plastic (FRP) Tubes as Energy Absorption Element in Vehicles, Energy Technology and Management, Prof. Tauseef Aized (Ed.), ISBN: 978-953-307-742-0, InTech, Available from: http://www.intechopen.com/books/energy-technology-and-management/a-study-on-design-of-fiber-reinforced-plastic-frp-tubes-as-energy-absorption-element-in-vehicles

INTECH
open science | open minds